Relamination Styles in Collisional Orogens

Petra Maierová, K. Schulmann, T. Gerya

AGU PUBLICATIONS

Tectonics

RESEARCH ARTICLE
10.1002/2017TC004677

Relamination Styles in Collisional Orogens

Petra Maierová[1,2], K. Schulmann[1,2], and T. Gerya[3]

[1]EOST, Institute de Physique de Globe, UMR 7516, Universite de Strasbourg, Strasbourg, France, [2]Center for Lithospheric Research, Czech Geological Survey, Prague, Czech Republic, [3]Institute of Geophysics, Department of Earth Science, ETH-Zurich, Zurich, Switzerland

Key Points:
- Presented numerical models of continental subduction and collision reproduce the relamination process for a range of conditions
- Relamination may occur directly into the crust for very weak overriding plates or through the overriding plate lithosphere
- Deep subduction and relamination through the overriding plate lithosphere is typical for quickly colliding young continents

Correspondence to:
P. Maierová,
petra.maierova@geology.cz

Citation:
Maierová, P., Schulmann, K., & Gerya, T. (2018). Relamination styles in collisional orogens. *Tectonics*, *37*, 224–250. https://doi.org/10.1002/2017TC004677

Received 25 MAY 2017
Accepted 29 NOV 2017
Accepted article online 14 DEC 2017
Published online 21 JAN 2017
Corrected 28 SEP 2018

This article was corrected on 28 SEP 2018. See the end of the full text for details.

Abstract During continental collision, a part of the lower-plate material can be subducted, emplaced at the base of the upper plate, and eventually incorporated into its crust. This mechanism of continental-crust transformation is called relamination, and it has been invoked to explain occurrences of high-pressure felsic rocks in different structural positions of several orogenic systems. In the present study we reproduced relamination during continental collision in a thermomechanical numerical model. We performed a parametric study and distinguished three main types of evolution regarding the fate of the subducted continental crust: (i) return along the plate interface in a subduction channel or wedge, (ii) flow at the bottom of the upper-plate lithosphere and subsequent translithospheric exhumation near the arc or in the back-arc region ("sublithospheric relamination"), and (iii) nearly horizontal flow directly into the upper-plate crust ("intracrustal relamination"). Sublithospheric relamination is preferred for relatively quick convergence of thin continental plates. An important factor for the development of sublithospheric relamination is melting of the subducted material, which weakens the lithosphere and opens a path for the exhumation of the relaminant. In contrast, a thick and strong overriding plate typically leads to exhumation near the plate interface. If the overriding plate is too thin or weak, intracrustal relamination occurs. We show that each of these evolution types has its counterpart in nature: (i) the Alps and the Caledonides, (ii) the Himalayan-Tibetan system and the European Variscides, and (iii) pre-Cambrian ultrahot orogens.

1. Introduction

"Relamination" is a part of the subduction and collision process where crustal material from the lower plate is emplaced—relaminated—at the base of the upper plate and eventually form a part of the upper plate (Chemenda et al., 2000; Hacker et al., 2011). The "relaminant" is formed generally by buoyant felsic metasedimentary or metaigneous rocks. Therefore, the relamination involves crustal "refinement" as it increases felsic composition of the bulk crust by separating felsic from mafic material, which is recycled into the mantle. Such a crustal refining is needed, because the primary continental crust is produced at island arcs, which implies mafic to intermediate lower-crustal composition (see overview by Kelemen et al., 2003). The existence of deeply subducted and relaminated felsic crust is further supported by the composition of ultra high pressure (HP) rocks exhumed at the surface (Schulmann et al., 2014; Yin et al., 2007) or by the character of deep crustal xenoliths trapped by volcanics (Ding et al., 2007; Hacker et al., 2000). These observations show that a significant proportion of the deep, and often HP, lower continental crust can be relatively felsic to intermediate (Hacker et al., 2011), in contrast to the commonly supposed mafic composition of the lower crust (Rudnick & Gao, 2003). Additional constraints from seismic studies and heat flow measurements are too weak to provide a clear answer on the lower-crust composition in most regions (Hacker et al., 2011).

The term relamination refers to the opposite process of delamination, during which a dense eclogitic crust and/or mantle separates from the overlying layers and sinks deeper into the mantle (e.g., Houseman & Molnar, 2001; Kay & Kay, 1993). Just as is suggested for delamination, relamination may have various forms and may involve metamorphic reactions, melting and melt separation (Kelemen & Behn, 2016). Classification of relamination types, depending on tectonic setting, was proposed by Hacker et al. (2011). One of the types is relamination during oceanic subduction when deeply subducted low-density sediments rise buoyantly, and along their exhumation path they may mix with the water enriched mantle and melt (e.g., Marschall & Schumacher, 2012). For their exhumation they can either exploit the subduction channel (e.g., Jolivet et al., 2003) or they can penetrate through the mantle wedge as diapirs and accumulate at the base of the lithosphere

or crust (e.g., Castro et al., 2013; Little et al., 2011). Another setting where relamination may occur is continental collision when a marginal part of a continent or a small continental block enters the subduction zone. Similar to sediments the continental crust may be exhumed along a subduction channel (Konopásek & Schulmann, 2005) or in the form of diapirs (Behn et al., 2011; Yin et al., 2007). Based on analogue models, it was proposed that a thick pile of continental crust may be detached from the subducting lithosphere and thrust backward along the subduction zone as a coherent sheet or relaminated near the crust-mantle boundary of the upper plate (Chemenda et al., 2000). In the latter case, thermal weakening of the relaminant due to the contact with the hot mantle can subsequently lead to its vertical exchange with the overlying dense material (Chemenda et al., 2000; Schulmann et al., 2014). Alternatively, if widespread melting of the subducted felsic material occurs, the rising melt can form plutons in the overlying plate (Tamura et al., 2010).

Understanding of relamination dynamics largely relies on numerical models (see, e.g., Hacker et al., 2011) that show how the deeply subducted felsic material can be exhumed back to crustal levels. Different settings have been modeled: exhumation of metasediments within the subduction channel (e.g., Gerya et al., 2002, 2008; Warren et al., 2008), penetration of sedimentary diapirs through the mantle wedge (e.g., Castro et al., 2013), and return of a subducted continental block along the subduction interface (Sizova et al., 2012). These models demonstrate the interplay between the plate motion and buoyancy during subduction and exhumation, and highlight the importance of rheology, namely, of deformation-, melt- and fluid-induced weakening on the tectonic evolution. However, relamination of substantial amounts of continental crust to the upper plate during collision, as evidenced, for example, in the Variscides (Schulmann et al., 2014) and Norwegian Caledonides (Johnston et al., 2007), has not been reproduced in numerical models so far and its dynamics is poorly understood. Besides that, a systematic numerical-modeling study of the relamination process in a postsubduction continental collision setting has been lacking since previous studies mainly focused on the relamination of oceanic crust and sediments by thermal-chemical plumes during oceanic subduction (e.g., Behn et al., 2011; Gerya & Yuen, 2003; Maunder et al., 2016; Zhu et al., 2009).

To fill this gap, we describe a series of models for continental collision and subduction that can be classified into three main groups according to the behavior of the deeply subducted crust: backflow in the subduction channel and formation of a collisional wedge, sublithospheric relamination and intracrustal relamination. The final objective of the paper is to show the role that selected parameters have on the model evolution and discuss the results with respect to characteristics of natural collisional zones.

2. Numerical Model Description

2.1. Method

The model simulates two converging continental plates initially separated by an oceanic domain which is being consumed at a subduction zone. As soon as the entire oceanic plate is subducted, the continental plates collide. The character of the collision, in particular, the fate of the continental crust of the lower plate, is the main focus of our study.

The model setup and parameter values are based on previous studies of subduction and collision that successfully reproduced the formation of (U)HP rocks (Dymkova et al., 2016; Faccenda et al., 2008; Sizova et al., 2012). The results of these models crucially depend on the incorporation of complex viscoplastic rheology, effect of fluids (water) and melt, which both reduce the strength of the rock, and major phase changes that affect the density. An important factor is the buoyancy of the crustal rocks, because it is the driving force for their exhumation. In our model we assume a rather simple parameterization of density and a relatively low density of the felsic crust relevant for relamination. We keep most of the material parameters fixed in order to obtain a manageable set of model cases and focus on the role of basic properties of the converging plates such as their velocity and lithospheric thickness.

The models are two-dimensional, and the model domain is 4,000 km wide and 1,000 km deep. In the domain, the equations of heat transport, motion, and continuity are solved, as specified in Appendix A. The equations are discretized and solved using a finite difference scheme on a fully staggered grid with variable resolution. The resolution is 1×1 km in a 1,500 km wide and 200 km deep region surrounding the contact between the subducting and overriding plates, and smoothly decreases to 5×10 km in the mantle far from this region. The particle-in-cell method is used to handle different types of material present in the domain. The initial density of the material particles (markers) is 28 particles per grid cell. The I2VIS software based on the work by Gerya and Yuen (2003) is used.

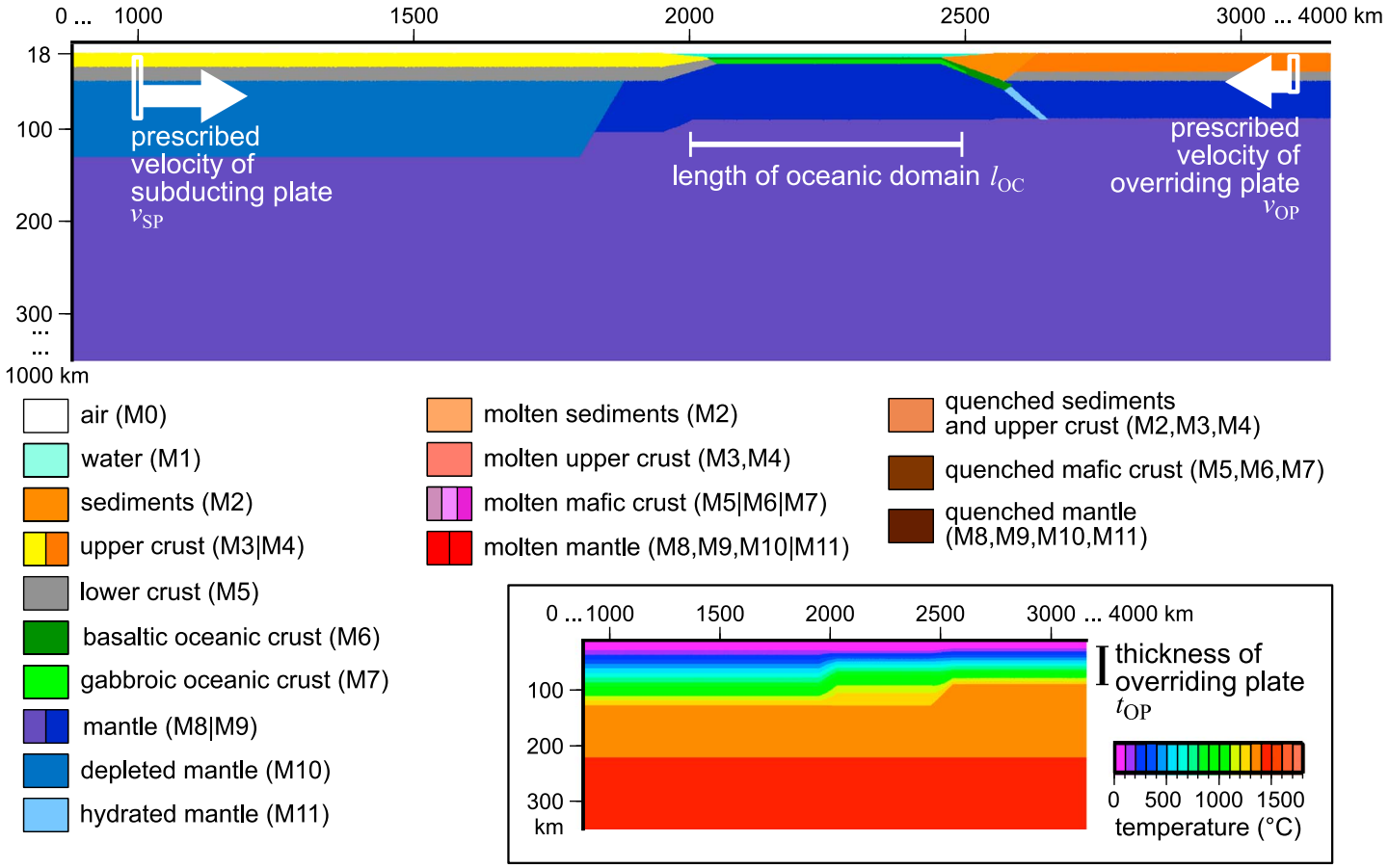

Figure 1. Initial material distribution and temperature field (inset) in the central part of the model domain. Full domain size is 4,000 × 1,000 km. Upper 18 km of the domain is initially filled with "sticky" air (material M0). Initial thicknesses of lithospheric layers are as follows: M3: 20 km; M4: 30 km (if not indicated differently); M5 in subducting plate: 15 km; M5 in overriding plate: 10 km (if not indicated differently); M6: 2 km; M7: 5 km; M10: 80 km. Properties of materials are in Tables 1 and 2. Arrows show regions where velocity is prescribed during the first stage of the evolution. In some models, the overriding plate has no fixed velocity. Temperature field in the continental lithosphere has a linear vertical gradient, in the oceanic lithosphere corresponds to the cooling geotherm. In the mantle below the lithosphere it continues with an adiabatic gradient of 0.5 K km^{-1} to 1790°C at 1,000 km depth.

2.2. Initial and Boundary Conditions

All domain boundaries are impermeable free slip. The deforming and stress-free surface of the Earth is approximated using "sticky air" (Crameri et al., 2012; Schmeling et al., 2008), a layer of low-density low-viscosity material representing air (M0) or water (M1) above the rock material. The interface between the "sticky air" and the "rock" is a surface where erosion and sedimentation operate (Gorczyk et al., 2007) (see also Appendix A).

The initial material distribution is depicted in Figure 1. The crust of the modeled continental plates consists of two layers: upper crust with felsic composition (M3, M4) and lower crust with mafic composition (M5). The oceanic crust consists of the upper basaltic (M6) and the lower gabbroic (M7) layers. The mantle (M8) and the lithospheric mantle (M9) differ only by temperature. The mantle lithosphere of the subducting continental plate (M10) is assumed to be depleted and therefore has a lower density. A sedimentary wedge is prescribed at the contact of the subducting and overriding plates. These sediments and the sediments that form later due to surface processes lubricate the subduction interface and facilitate the relative motion of the plates. In addition, a zone of weak hydrated mantle (M11) is initially prescribed at the subduction interface.

The convergence of the plates is induced by the velocity prescribed at $x = 1{,}000$ km (subducting plate) and $x = 3{,}100$ km (overriding plate) (see Figure 1). At the left and right model boundaries, weak regions in the lithosphere are prescribed where the deformation due to the plate motion is accommodated. The convergence rate is fixed only during the first stage of the model evolution. Afterward, the subduction and collision continue freely and are governed by the buoyancy forces in the crust and mantle. The rate of convergence and duration of the convergence conditions vary between models as specified in Table 3.

Table 1
Values of Model Parameters

Symbol	Meaning	Value, unit
α	thermal expansivity	$2 \cdot 10^{-5}\,K^{-1}$; zero in air and water (M0, M1)
β	compressibility	$4.5 \cdot 10^{-4}$; zero in air and water (M0, M1)
C	cohesion	1 MPa
c_p	heat capacity	1,000 J kg^{-1}K^{-1}
ϵ_0	initial strain for weakening	0
ϵ_1	final strain for weakening	1
η_{min}	minimum viscosity	10^{18} Pa s; 10^{17} Pa s in air and water (M0, M1)
η_{max}	maximum viscosity	10^{26} Pa s
H_L	latent heat of melting	— kJ kg^{-1}; see Table 2
H_r	radiogenic heat sources	— W m^{-3}; see Table 2
λ_f	fluid-induced weakening coefficient	10^{-2}
λ_m	melt-induced weakening coefficient	10^{-3}; 10^{-2} in models 35 and 36
k	thermal conductivity	$(k_0 + k_1/(T_{(K)} + 77))\exp(4 \cdot 10^{-11} P_{(Pa)})$ W m^{-1} K^{-1}; see Table 2
l_{OC}	length of oceanic plate	700 km except models 23–26; see Table 3
ρ_0	reference density	— kg m^{-3}; see Table 2
T_{min}	temperature for kinetics of phase transition	400°C; 600°C in lower crust (M5)
T_{max}	temperature for kinetics of phase transition	600°C; 800°C in lower crust (M5)
T_0	reference temperature	0°C
T_{liquid}	liquidus temperature	— K; see Table 2
T_{solid}	solidus temperature	— K; see Table 2
$T_{w,max}$	maximum temperature for water in rock	1,700 K
X_{min}	unextractable melt fraction	0.01
X_{max}	maximum melt fraction retained in rock	0.02
X_{w0}	initial fluid content in rock	— wt %; see Table 2
ϕ_0	initial internal friction coefficient	— ; see Table 2
ϕ_1	final internal friction coefficient	— ; see Table 2
t_{OP}	thermal thickness of overriding plate	50–110 km; see Table 3
t_{SP}	thermal thickness of subducting plate	110 km; 70 km in model 34
v_{w0}	velocity of percolating water	10 cm yr^{-1}
v_{OP}	velocity of overriding plate	0 cm yr^{-1} except models 31–32; see Table 3
v_{SP}	velocity of subducting plate	3–6 cm yr^{-1}; see Table 3
$y_{w,max}$	maximum depth for water in rock	150 km

Temperature is fixed at the top and bottom boundaries to 0° C and 1790° C, respectively. Zero heat flux is prescribed on sides. The initial temperature (Figure 1) corresponds to a combination of continental or oceanic geotherm in the lithosphere and adiabatic gradient deeper in the mantle.

2.3. Material Properties

The model domain contains several distinct materials which can have different properties such as density, viscosity parameters, conductivity, and latent heat of melting. The list of material parameters and their values are in Tables 1 and 2.

The density of solid material depends on composition, temperature, and pressure:

$$\rho_{PT} = \rho_0 \left[1 - \alpha(T - T_0)\right] \left[1 + \beta(P - P_0)\right] \chi_\rho, \tag{1}$$

where ρ_0 is the reference density at the temperature $T = T_0$ and pressure $P = P_0$, α is the thermal expansivity, and β is the compressibility. The coefficient χ_ρ represents density changes due to phase transitions induced by pressure and temperature changes. We assume that the mafic crust (material M5–M7) is affected by the

Table 2
Material Properties

Material (ID)	ρ_0 (kg m^{-3})	X_{w0} wt %	η_{eff} Flow law	T_{solid} (K)	T_{liquid} (K)	$\phi_0-\phi_1$	H_L (kJ kg^{-1})	H_r (μW m^{-3})	k_0 (W m^{-1} K^{-1})	k_1 (W m^{-1})
Air (M0)	1	—	10^{17} Pa s	—	—	0–0	—	—	200	0
Water (M1)	1,000	—	10^{17} Pa s	—	—	0–0	—	—	200	0
Sediments (M2)	2,900[a]	2	wet quartz	—[b]	—[f]	0.3–0.15	300	2.0	0.64	807
Felsic crust (M3, M4)	2,700	0	wet quartz	—[c]	—[f]	0.6–0.3	300	1.0	0.64	807
Mafic crust (M5)	3,000	0	anorthite	—[d]	—[d]	0.6–0.3	380	0.25	1.18	474
Basalt (M6)	3,000	2	wet quartz	—[e]	—[d]	0.6–0.3	380	0.25	1.18	474
Gabbro (M7)	3,000	0	anorthite	—[d]	—[d]	0.6–0.3	380	0.25	1.18	474
Molten M2	2,400	2	wet quartz	—	—	0–0	300	2.0	0.64	807
Molten M3, M4	2,400	2	wet quartz	—	—	0–0	300	1.0	0.64	807
Molten M6	2,400	2	wet quartz	—	—	0–0	380	0.25	1.18	474
Molten M5, M7	2,900	2	anorthite	—	—	0–0	380	0.25	1.18	474
Mantle										
– Dry (M8, M9)	3,300	0	dry olivine	—[g]	—[g]	0.6–0.3	400	0.022	0.73	1,293
– Depleted (M10)	3,250	0	dry olivine	—[g]	—[g]	0.6–0.3	400	0.022	0.73	1,293
– Hydrated (M11)	3,300	2	wet olivine	—[g]	—[g]	0.3–0.15	400	0.022	0.73	1,293
Molten M8–M11	2,900	2	dry olivine	—	—	0–0	400	0.022	0.73	1,293

Note. Flow law parameters are listed in Appendix A. Latent heat of melting is according to Bittner and Schmeling (1995) and Turcotte and Schubert (2002). Conductivity parameters are according to Clauser and Huenges (1995).
[a]ρ_0 is increased assuming peraluminous composition and high garnet content in deeply subducted metasediments. [b]Poli and Schmidt (2002) for sediments. [c]Poli and Schmidt (2002) for sediments increased by 200 K (except for model 37). [d]Hess (1989). [e]Poli and Schmidt (2002) for mid-ocean ridge basalt. [f]Johannes (1985). [g]Mantle melting is calculated using the approach by Katz et al. (2003).

transformations of basalt to garnet granulite and eclogite (Ito & Kennedy, 1971), and spinel to perovskite (Ito et al., 1990; Mishin et al., 2008). Phase transformations in the felsic rocks (M2–M4) are neglected, because they are strongly dependent on composition, which is highly variable in nature. In the mantle (M8–M11), transformations of olivine to spinel and perovskite are taken into account (Ito et al., 1990; Katsura & Ito, 1989). At low temperatures ($T < T_{max}$), slow reaction kinetics hinder the phase transitions: $\chi_\rho = 1$ for $T < T_{min}$ and χ_ρ varies linearly from 1 to the kinetics-independent value between $T = T_{min}$ and $T = T_{max}$.

We use the viscoplastic rheology of the material expressed using the effective viscosity η_{eff}, as described in Appendix A. The viscous (ductile) behavior is prescribed as a combination of dislocation, diffusion, and Peierls creep (for mantle rocks) using their respective viscosities η_{dis}, η_{dif}, and η_{pei}:

$$\eta_d = \min\left[\left(1/\eta_{dis} + 1/\eta_{dif}\right)^{-1}, \eta_{pei}\right]. \quad (2)$$

The plasticity approximates the brittle failure of the rock. It occurs when the second invariant of the stress tensor σ_{II} reaches the yield strength σ_y, and it limits the effective viscosity as

$$\eta_{eff} = \min\left(\eta_d, \frac{\sigma_y}{\dot{\epsilon}_{II}}\right), \quad (3)$$

where $\dot{\epsilon}_{II}$ is the second invariant of the strain rate tensor. The yield strength is prescribed using the Drucker-Prager criterion:

$$\sigma_y = C + \phi P_{eff}, \quad (4)$$

where C is the cohesion and ϕ is the internal friction coefficient, which can depend on the total plastic strain. We assume that it decreases linearly from the initial to the final value between the plastic strain ϵ_0 and ϵ_1 (see Table 1). P_{eff} is the effective pressure which equals dynamic pressure P for solid rocks without free water and is modified in the presence of fluids or melt (see the following section).

2.4. Hydration, Melting, and Melt Extraction

We use a highly simplified linear slab dehydration model (Gerya et al., 2002). Some materials contain a certain wt % of water (X_{w0}) at the beginning of the model evolution. The maximum water content that can be retained in the rock decreases with pressure and temperature due to compaction and dehydration reactions:

$$X_w = X_{w0}\,\frac{T_{w,\max} - T}{T_{w,\max} - T_0}\,\frac{y_{w,\max} - y + y_e}{y_{w,max}} \tag{5}$$

where the y coordinate increases downward and corresponds to the depth, $T_{w,\max}$ and $y_{w,\max}$ are maximum temperature and depth, respectively, at which water can be retained in the rock, and y_e is the vertical position of the surface (Gerya et al., 2002).

The excess water is released as a fluid particle that migrates with a velocity of

$$\begin{aligned} v_{wx} &= v_x, \\ v_{wy} &= v_y - v_{w0}, \end{aligned} \tag{6}$$

where v_{w0} is the prescribed relative velocity of water with respect to the rock (Vogt et al., 2012). It migrates until it reaches material that can consume an additional amount of water according to equation (5). We assume that below a certain depth ($y_{w,\max}$) no free water can exist and all fluid particles are removed.

The amount of melt produced by the material depends on pressure, temperature, and water content. For crustal materials, the melt content is calculated using solidus and liquidus temperatures, T_{solid} and T_{liquid}, respectively. The volumetric fraction of melt X_{m0} produced by the rock increases linearly between T_{solid} and T_{liquid}:

$$\begin{aligned} X_{m0} &= \frac{T - T_{solid}}{T_{liquid} - T_{solid}} \text{ if } T_{solid} < T < T_{liquid}, \\ X_{m0} &= 0 \text{ if } T < T_{solid}, \\ X_{m0} &= 1 \text{ if } T > T_{liquid}. \end{aligned} \tag{7}$$

The adopted parameterization of solidus and liquidus temperatures is based on experimentally determined melting relations (Hess, 1989; Johannes, 1985; Poli & Schmidt, 2002; Table 2) fitted by analytical functions of pressure (Sizova et al., 2012). For the mantle melting, we adopted a more complex approach by Katz et al. (2003).

The melt fraction in the rock X_m depends on the total extracted melt during the previous evolution $\sum X_{ext}$:

$$X_m = X_{m0} - \sum X_{ext}. \tag{8}$$

Only a limited amount of melt can remain in the source rock. Once the melt fraction X_m exceeds the threshold X_{max}, a part of the melt $X_{ext} = X_m - X_{min}$ is released while a fraction X_{min} remains in the source rock. A part of the water proportional to X_{ext} is assumed to be extracted together with melt and therefore removed from the rock.

Melt is extracted in batches represented by melt particles. Migration of melt is assumed to be instantaneous in the model time scale and independent of solid material deformation (Nikolaeva et al., 2008). The melt particles are therefore emplaced above the site of melt extraction, where they form either volcanic or plutonic rocks. Volcanics form just below the surface, while plutonic rocks are emplaced at a larger depth in the site of the highest intrusion emplacement rate div_{crust} determined by evaluating locally the ratio of the effective melt overpressure to the effective viscosity of the crust (Vogt et al., 2012):

$$\mathrm{div}_{crust} = \left(P_{melt} - g\rho_{melt}(y - y_{melt}) - P\right)/\eta_{crust}, \tag{9}$$

where P_{melt} and P is the pressure at the extraction level y_{melt} and at the crustal level y, respectively, g is the gravitational acceleration, ρ_{melt} is the melt density, and η_{crust} is the effective local crustal viscosity at the level y. The effects of matrix compaction in the melt extraction area and crustal divergence in the melt emplacement area are taken into account in the compressible continuity equation (A1).

Both fluid and melt presence affect the effective viscosity and density of the rock. Hydrated mantle ($X_w > 0$) and molten rocks ($T > T_{solid}$) deform according to different flow laws and with a lower internal friction (Table 2). In addition, the presence of markers representing percolating fluids decreases the effective pressure in the definition of the yield strength (4): $P_{eff} = P\lambda_f$, where λ_f is a constant coefficient, $0 < \lambda_f < 1$. Similarly, during a melt extraction episode, P_{eff} in the column between the source of the melt and the surface is decreased according to $P_{eff} = P\lambda_m$, $0 < \lambda_m < 1$.

The effective density ρ_{eff} of partially molten rocks is calculated from

$$\rho_{eff} = \rho_{PT,solid} + X_m \left(\rho_{PT,molten} - \rho_{PT,solid}\right), \tag{10}$$

where $\rho_{PT,solid}$ and $\rho_{PT,molten}$ are the densities of solid and molten rock, respectively, according to (1). The effects of latent heating are accounted for by an increased effective heat capacity $c_{p,eff}$ and thermal expansion α_{eff} of the partially molten rocks, calculated as (Gerya et al., 2008)

$$c_{p,eff} = c_p + H_L \left(\frac{\partial X_m}{\partial T}\right)_P,$$
$$\alpha_{eff} = \alpha + \frac{\rho H_L}{T} \left(\frac{\partial X_m}{\partial P}\right)_T, \tag{11}$$

where c_p and α are the heat capacity and the thermal expansion of the solid rock, respectively, and H_L is the latent heat of melting (Table 1).

3. Results

3.1. Model Cases and Varied Parameters

We study a series of models with different parameters defined in Table 3. The principal varied parameters are the age of the oceanic domain, the velocity of the subducting plate, and the thermal thickness of the overriding plate. In addition, we test the influence of the length of the oceanic domain, thickness of the subducting plate, the strength of the overriding plate (thickness of the lower crust), melt weakening (λ_m), and boundary conditions (nonzero velocity of the overriding plate, fixed versus free motion of the overriding plate, and initial location of the trench).

The prescribed parameters of the oceanic lithosphere (convergence velocity and initial age) are based on data for natural subduction zones (Jarrard, 1986), even if the tested values do not cover the whole range of observed values. The initial age of the oceanic lithosphere of 20, 30, and 40 Myr, and lengths of 500 and 700 km are tested. The tested plate convergence velocities of 3, 4 and 6 cm yr^{-1} represent relatively slow, moderate and fast subductions, respectively. In total it gives the ages of the oceanic plate at the onset of collision between 38 and 63 Myr (see Table 3).

On Earth, the thickness of the continental lithosphere varies between ~50 km in rifted domains and >250 km in cratons (Artemieva, 2006). Here we focus on relamination, which, as demonstrated further in our study, is more likely to occur in the case of a thin overriding plate. It is therefore sufficient to test relatively low values for this thickness: 50, 70, 90, and 110 km.

For different combinations of parameter values we obtain a wide spectrum of evolution styles. In section 3.2 we describe the representative models for the main types of evolution that repeatedly occur for different combinations of model parameters. In section 3.3 we show the role of selected parameters in the evolution of the model.

3.2. Fate of Subducted Continental Crust in Models

The initial phase of evolution covering most of the oceanic subduction is similar in all modeled cases (Figure 2). During oceanic subduction, water contained in the oceanic crust is gradually released, percolates upward, and hydrates a thin layer of the mantle just above. A part of the hydrated mantle melts, because its melting temperature decreases with water content. At the trench, a part of the sediments are dragged by the oceanic crust into the subduction zone, while the rest forms a wedge at shallow levels. The subducting sediments are also partially molten, and the released melt rises and weakens the mantle wedge and the overriding plate.

AGU Tectonics

10.1002/2017TC004677

Table 3
Model Cases

Model ID	Duration of convergence condition (Myr)	Initial ocean age (Myr)	Ocean age at beginning of collision (Myr)	OP thickness (km)	Additional parameters	Horizontal flow in:	Exhumation near: A = arc, B = backarc, I = plate interface	Plate interface and OP crust deformation	Style
1	18	20	38	50		crust	—	ductile thickening	C
2	30	20	38	50		crust	—	ductile thickening	C
3	18	30	48	50		crust	—	ductile thickening	C
4	30	30	48	50		crust	—	ductile thickening	C
5	18	40	58	50		crust	—	ductile thickening	C
6	30	40	58	50		crust	—	ductile thickening	C
7	18	20	38	70		—	I	separation of fore-arc block	w
8	30	20	38	70		mantle	B I	disruption in back arc, one major thrust	L-S/W
9	18	30	48	70		—	I	extension at trench, weak OP deformation	W
10	30	30	48	70		—	A I	extension at trench, separation of fore arc	L-W
11	18	40	58	70		—	I	extension at trench, steep thrusts	W
12	30	40	58	70		mantle	I	extension at trench, steep thrusts	S/W
13	18	20	38	90		—	I	extension at trench, weak OP deformation	s
14	30	20	38	90		mantle	B I	disruption and extension in back arc	L-s/w
15	18	30	48	90		—	I	extension at trench and arc	s
16	30	30	48	90		mantle	I	weak OP deformation	s/w
17	18	40	58	90		—	I	extension at trench, weak deformation	s
18	30	40	58	90		mantle	I	weak OP deformation	S
19	18	20	38	110		—	I	wide extension near trench, weak OP deformation	s
20	30	20	38	110		mantle	I	weak OP deformation	S
21	18	30	48	110		—	I	extension at trench, weak deformation	s
22	30	30	48	110		mantle	I	weak OP deformation	s/w
23	13	40	53	70	l_{OC} = 500 km	(crust)	A I	separation of fore-arc block	L-s/w
24	25	40	53	70	l_{OC} = 500 km	mantle	B I	steep thrusts, disruption in back arc	L-s/w
25	17	40	57	70	l_{OC} = 500 km,	(crust)	A I	separation of fore-arc block	L-s/w
26	33	40	57	70	l_{OC} = 500 km, v_{SP} = 3 cm yr^{-1}	mantle	B	disruption in back arc, one major thrust	L

AGU Tectonics

Table 3 *(continued)*

Model ID	Duration of convergence condition (Myr)	Initial ocean age (Myr)	Ocean age at beginning of collision (Myr)	OP thickness (km)	Additional parameters	Horizontal flow in:	Exhumation near: A = arc, B = backarc, I = plate interface	Plate interface and OP crust deformation	Style
27	24	40	63	70	$v_{SP} = 3$ cm yr^{-1}	—	I	extension near trench, weak OP deformation	W
28	40	40	63	70	$v_{SP} = 3$ cm yr^{-1}	mantle	I	extension near trench, steep thrusts	W
29	12	40	52	70	$v_{SP} = 6$ cm yr^{-1}	(crust)	A	separation of fore-arc block	L
30	20	40	52	70	$v_{SP} = 6$ cm yr^{-1}	(crust)	A I	separation of fore-arc block	L-s/w
31	30	40	58	70	free OP	(crust)	A	separation of fore-arc block	L
32	30	40	58	70	$v_{SP} = 3$ cm yr^{-1}, $v_{OP} = 1$ cm yr^{-1}	(crust)	A	separation of fore-arc block	L
33	30	40	58	70	trench at $x = 2250$ km	mantle	B I	disruption in back arc, one major thrust	L-s/w
34	30	40	58	70	$t_{SP} = 70$ km	mantle	B I	disruption in back arc, steep thrusts	L-s/w
35	30	20	38	70	$\lambda_m = 10^{-2}$	mantle	I	weak OP deformation	s
36	30	40	58	70	$\lambda_m = 10^{-2}$	(crust)	A	separation of fore-arc block	L
37	30	20	38	70	T_{solid} in M3 same as in M2	mantle	B	disruption in back arc, one major thrust	L
38	30	20	38	70	M5 in OP 5 km thick	crust	—	ductile thickening	I
39	30	40	58	70	M5 in OP 5 km thick	—	I	extension at trench, steep thrusts	S/W

Note. Default Parameters: $l_{OC} = 700$ km, $v_{SP} = 4$ cm yr^{-1}, $v_{OP} = 0$ cm yr^{-1}. OP = overriding plate; SP = subducing plate; style: L = sublithospheric relamination, C = intracrustal relamination, S = subduction channel, W = collisional wedge. Size of the channel or wedge is indicated by lower or upper case.

10.1002/2017TC004677

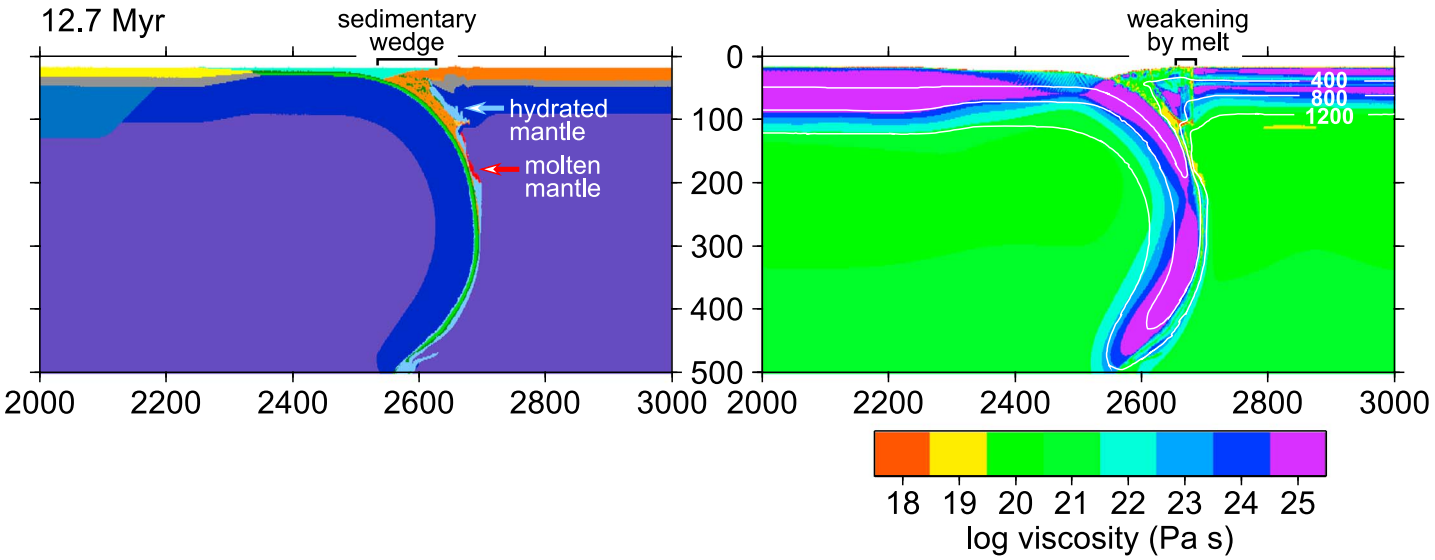

Figure 2. Initial stage of the model evolution: oceanic subduction and formation of the magmatic arc (model 12). (left) Material distribution, (right) viscosity and isotherms in a representative time step. Color coding of materials is shown in Figure 1. Labels of isotherms are in degrees Celsius. For details see text.

The oceanic plate is bent to a nearly vertical direction in the upper mantle. The bending of the lithosphere is accommodated by normal faulting in the outer rise area left of the trench. At deeper levels, the deformation of the cold slab is negligible except at ~200 km depth where it unbends and at the relatively warm slab tip.

The subsequent collision-related evolution differs for different model cases, but most of them resemble one of the models described in the following sections 3.2.1 – 3.2.4

3.2.1. Deep Subduction and Exhumation Near Continental Magmatic Arc

In the first type of models (Figure 3), the melt from the hydrated mantle, subducted crust, and sediments forms a magmatic arc ~150 km right of the trench and weakens the overriding plate in this region. The weakened zone can be easily deformed, and the stress induced by slab pull and trench retreat leads to the opening of a vertical channel through the crust. The partially molten sediments and subsequently the subducted felsic continental crust use this channel for their exhumation (top and middle rows in Figure 3).

The fore-arc region has a high viscosity and is only weakly deformed. The lithosphere behind the arc bends downward due to the ongoing convergence of the continental plates. The crustal part of the back arc thickens as it is being filled by the exhumed felsic material — "the relaminant" (bottom row in Figure 3). The resulting thick pile of felsic material gradually warms up due to radiogenic sources and weakens mainly at the lower crustal level. The low-viscosity lower crust flows horizontally, and simultaneously, a topographic plateau forms above it. With an increasing temperature, parts of the lower and middle crust melt. Eventually, a second exhumation event takes place along the plate interface. Maximum temperatures recorded by the relaminant that was exhumed at midcrustal or shallower levels are around 700°C and are achieved during its residence in the crust after the exhumation.

The typical configuration during mature collision is (from left to right) weakly deformed subducting plate; back-thrust continental material and remnants of the sedimentary wedge; weakly deformed upper-plate lithospheric block with preserved low-grade rocks; felsic body near the former magmatic arc; thick warm and weak crust in the back-arc region penetrated by magmatic rocks; and weakly deformed overriding plate.

3.2.2. Deep Subduction and Exhumation Through Continental Back Arc

In some models (Figure 4), the felsic crust and sediments reach a depth of >100 km below sea level before they mechanically detach from the more mafic layers of the subducting plate (top row in Figure 4). For a thin overriding plate this depth corresponds to the bottom of the lithosphere. The exhumation of the felsic material at this level is hindered by the strong lithosphere above but it can flow laterally forming a long sheet. It gradually warms up due to the contact with the surrounding hot mantle and reaches temperatures of up to 800°C at this stage. This temperature is significantly lower than that of the mantle because the volume of the subducted material is large and its residence in the mantle is relatively short (about 5 Myr). Its peripheral

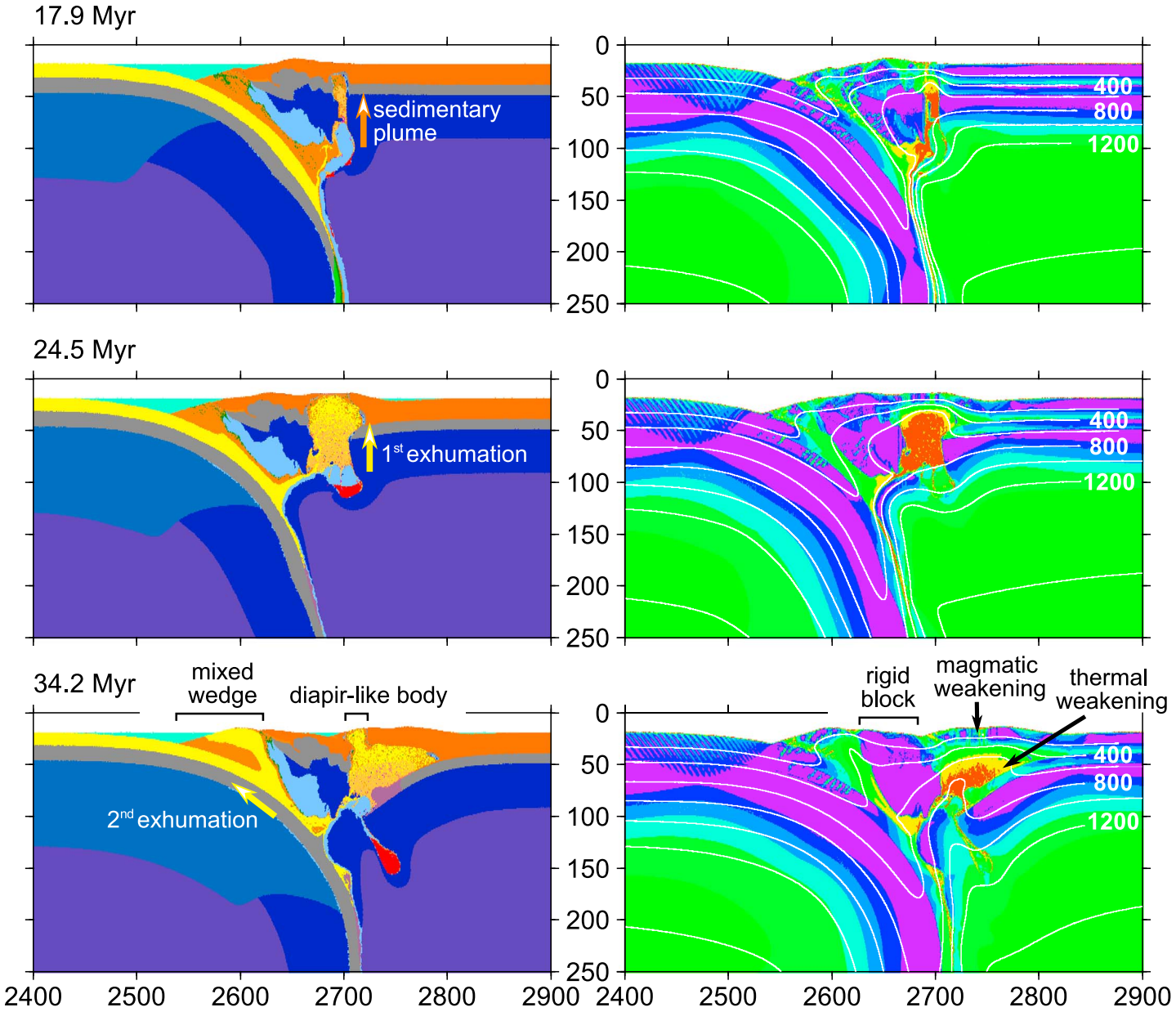

Figure 3. Exhumation through the overriding-plate lithosphere near the magmatic arc (model 23). Color scales and figure layout except the size of the plotted domain are the same as in Figure 2. For details see text.

parts partially melt, and at ~32 Myr (~14 Myr after the beginning of the collision) the total amount of extracted melt X_m locally reaches 30%. Melting occurs only in the sedimentary material (M2) which has lower solidus temperature than the continental felsic material (M3) in this case. The uprising melt weakens the column of the lithosphere above, and eventually, quick translithospheric exhumation of the relaminant occurs through the weakened zone all the way to the crust (middle row in Figure 4). The second exhumation event occurs along the contact of the plates and evacuates the rest of the felsic material from below the overriding lithosphere (bottom row in Figure 4).

In the overriding plate, the ongoing compression is accommodated by bending of the mantle lithosphere, thickening of the crust in the root domain, and its shallow thrusting over the external lithosphere. Subsequently, the lower part of the relaminant flows horizontally forming a wide lower- to middle-crustal pillow (bottom row in Figure 4).

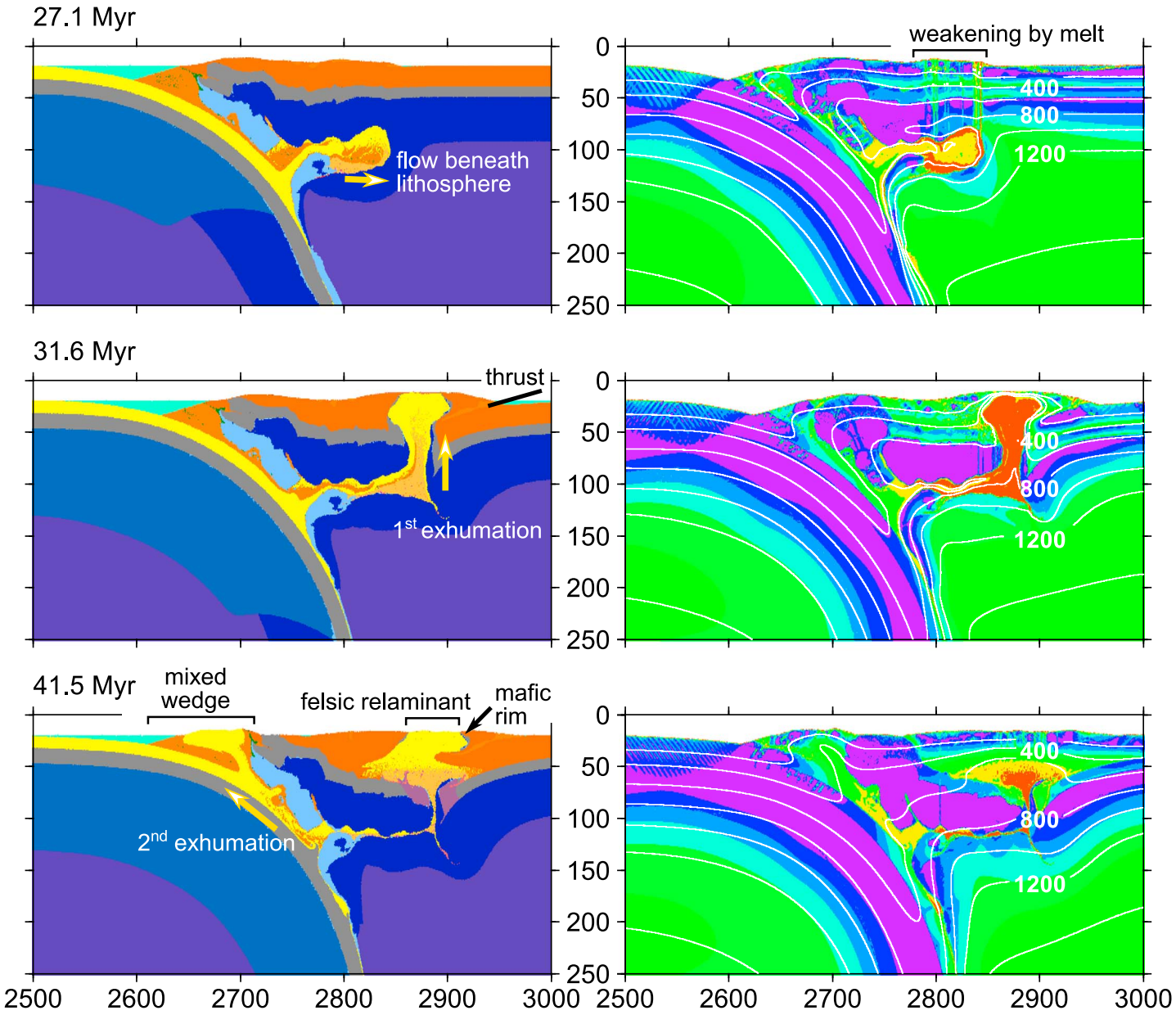

Figure 4. Exhumation through the overriding-plate back-arc lithosphere (model 8). Color scales and figure layout are the same as in Figure 3. For details see text.

The typical configuration is similar as in the previous case, but the exhumed relaminant is spatially separated from the volcanic arc. In addition, it is rimmed by mafic lower-crustal material that witnesses its penetration through the mantle and lower crust. Deformation of the upper crust is localized into a prominent flat thrust at the right margin of the collisional area, and the rest of the plate right of the thrust is practically undeformed.

3.2.3. Exhumation Near Contact of Plates

For various reasons, deep subduction of the felsic material and/or its relamination into the upper plate can be limited (Figures 5 and 6).

The first example of this behavior is a model where an imbalance between the plate velocities and the strong slab pull causes extension in the trench area (Figure 5). The extension is accompanied by melting and formation of small upwellings of partially molten sediments which altogether form a weak fore-arc region. After the arrival of the continent, the felsic continental crust preferentially intrudes this weak region, while only a small part subducts deeper. The final configuration shows three distinct regions: the weakly deformed subducting

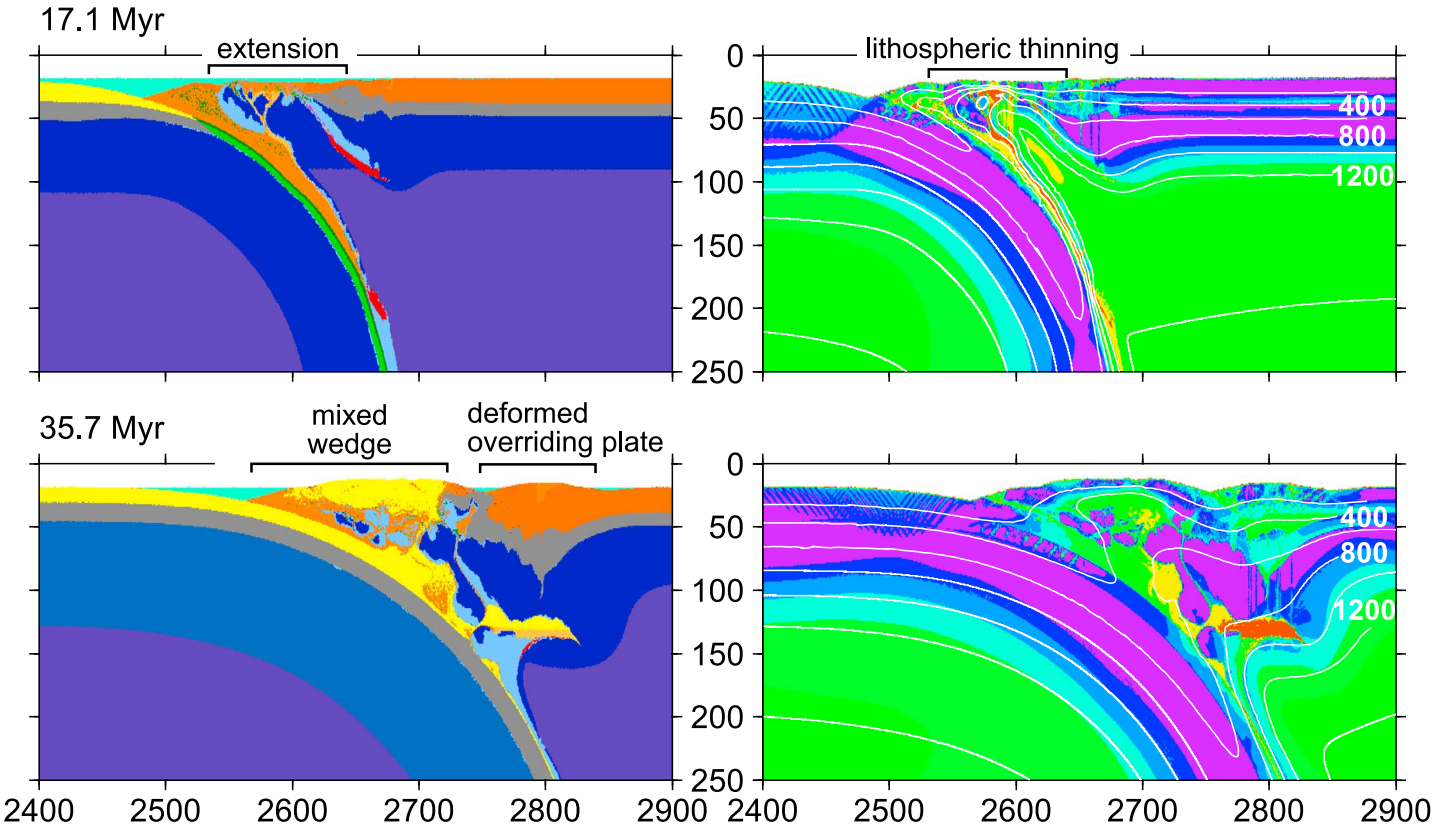

Figure 5. Extension and thinning near the contact of plates resulting into formation of the collisional wedge (model 12). Color scales and figure layout are the same as in Figure 2. For details see text.

plate, the back-thrust continental material and sediments with peak temperatures ~600°C, and the weakly to moderately deformed overriding plate.

A similar final geometry can be achieved via a completely different evolution (Figure 6). Initially, the felsic crust is subducted below lithosphere similar to the situation in Figure 4 forming a long sheet of partially molten rocks. However, the overriding plate is too strong and therefore the relaminant cannot penetrate through it and exhume vertically. As a result, the material is extruded back and finally exhumed along the subduction interface via a weak hot channel. The maximum recorded temperatures (~700°C) are slightly lower than in the case of the complete subduction-relamination history, but maximum pressures are practically the same. A significant part of the relaminant remains stacked at the bottom of the upper-plate lithosphere until the end of the simulation, that is, at least 30 Myr after the beginning of the collision. The stacked material thermally equilibrates with the mantle—the isotherms become almost horizontal in this region.

3.2.4. Inflow Into Overriding-Plate Crust

In the last distinct class of models the relaminant remains at the crustal level and flows directly into the overriding-plate middle and lower crust in a form of a long horizontal channel (Figure 7). The maximum depth reached by the felsic crust is ~80 km, but typically it reaches ~60 km below sea level or less.

The overriding plate has to be extremely weak, for example, due to high-temperature gradient, to permit such behavior. In such a case, the convergence of the continental plates induces shortening and thickening of the overriding plate and formation of a wide topographic plateau. The thickening is mostly accommodated in the weak middle and lower crust that is dominated by the relaminated material including sediments and pieces of oceanic crust. The mafic lower crust and lithospheric mantle deform by intensive folding. Importantly, as there is no significant difference in densities between the relaminant and the upper plate crust, the buoyancy-driven exhumation does not take place.

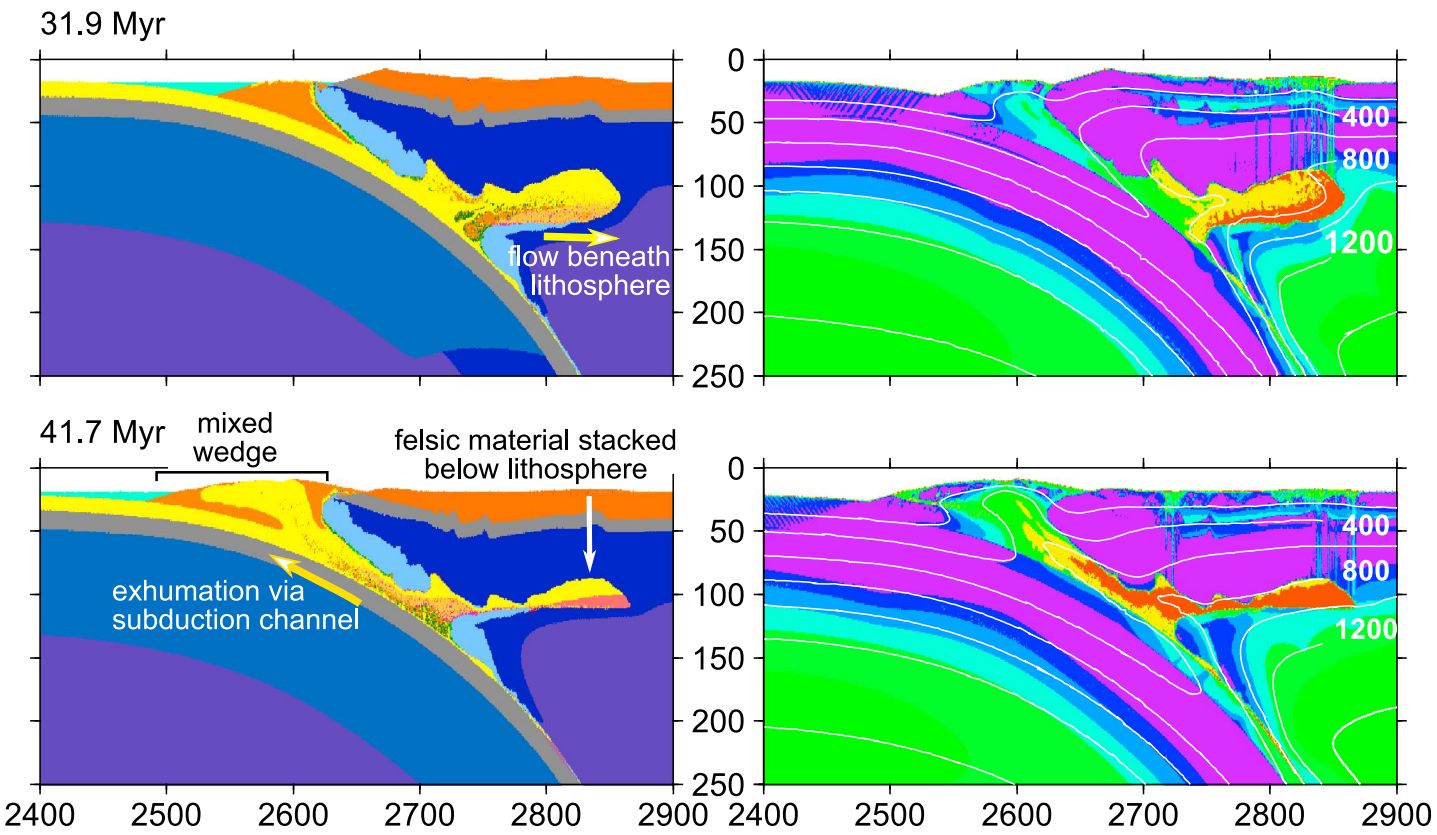

Figure 6. Exhumation along the contact of plates via the subduction channel (model 18). Color scales and figure layout are the same as in Figure 2. For details see text.

3.3. Effect of Model Parameters

The contrasting model evolutions can be obtained in the same general setup by simple modifications of the parameter values. In Table 3 we describe the model cases using the following key features: presence of horizontal flow of the subducted continental crust (in crust, in sublithospheric mantle, or none), the site of exhumation of the subducted continental crust (near arc, in back arc, near plate interface, or none), and dominant deformation of the overriding plate and vicinity of the plate interface (e.g., extension near trench, separation of fore-arc block, disruption of lithosphere in back arc, multiple thrusts or one major thrust, ductile thickening, or weak overriding plate deformation). In the last column of Table 3 we classify the models according to these features into the following three major types:

1. The first type of model evolution is called here the sublithospheric relamination (marked "L" in Table 3). Subduction of the continental material beneath the overriding plate lithosphere and its exhumation either near the magmatic arc (as in Figure 3) or in the back arc (as in Figure 4) are characteristic for this type. Disruption near the arc and the separation of a rigid fore-arc block, or disruption in the back arc accompany the exhumation. In the case of exhumation in the back arc, it is typical for horizontal flow in the sublithospheric mantle to temporarily form a long sheet of continental material. Some models show also horizontal flow of the relaminant in the crust after exhumation.
2. The second group of models is characterized by exhumation near the plate interface in the form of a subduction channel (as in Figure 5, marked "S") or a collisional wedge (as in Figure 6, marked "W"). The distinction between the channel or wedge is rather subjective. We mostly rely on the overall shape of the exhumed crustal body and on the path of exhumation (parallel to the plate interface or more complex in the case of the channel or wedge, respectively). Extension near the trench and concentration of deformation in this region commonly leaves the rest of the overriding plate relatively weakly deformed in this type of evolution, but thrusting related to compression may be also present.

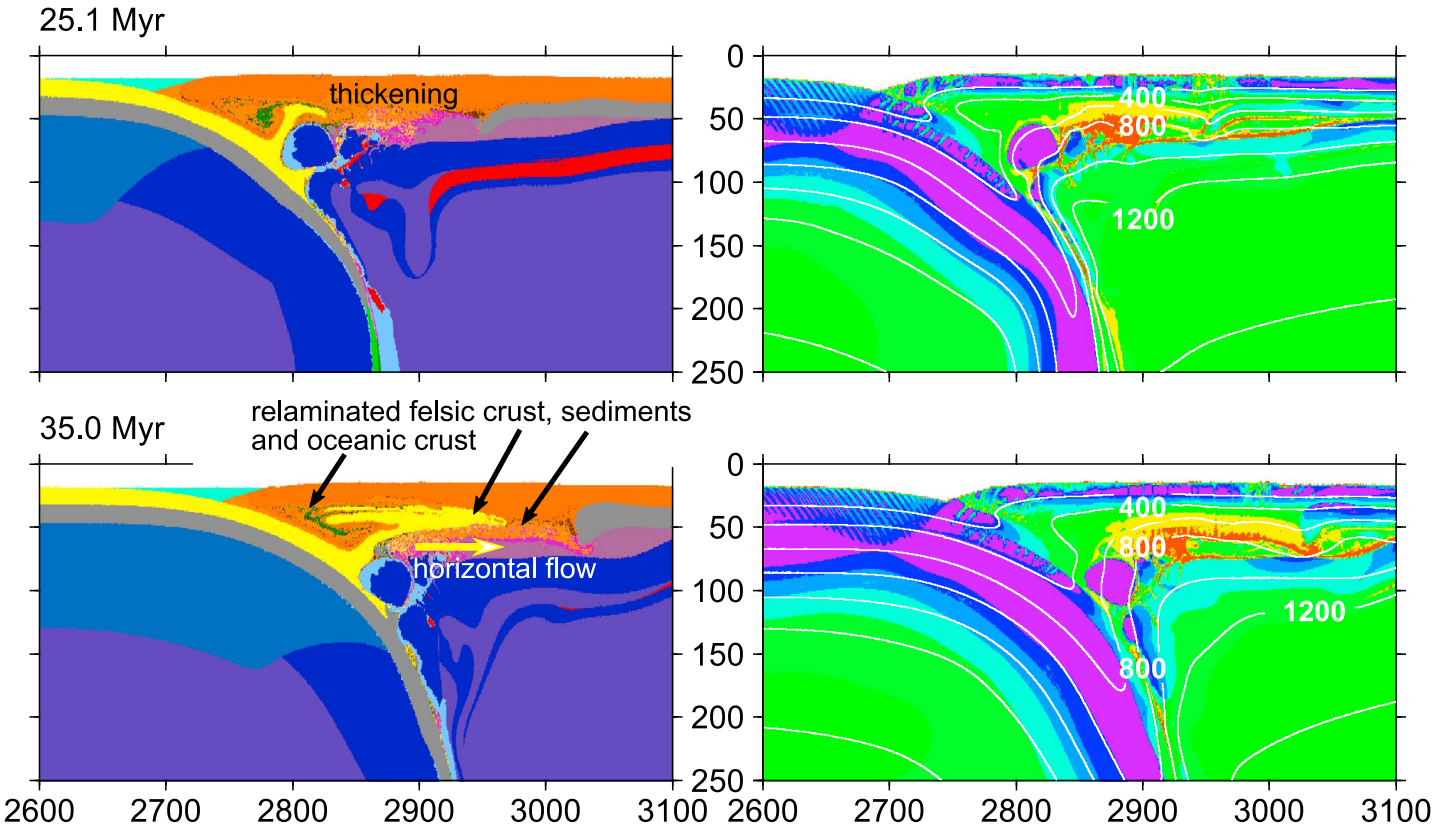

Figure 7. Horizontal flow into the thickened overriding-plate crust (model 1). Color scales and figure layout are the same as in Figure 2. For details see text.

3. In the last type of model the crust of the subducting plate flows mostly horizontally directly into the crust of the overriding plate (as in Figure 7, marked "C") and is called here the intracrustal relamination. It is associated with ductile thickening of the crust of the overriding plate.

The different styles of evolution can be combined in a single model if multiple exhumation events occur (e.g., "L-W" as in model 10).

The results summarized in Table 3 and Figure 8 document the impact of the model parameters on the development of these styles. The first observation is that the kinematically prescribed velocity has a dominant effect on the subduction and relamination of the continental crust. If the kinematic condition is switched off at the beginning of the continental collision (models 1, 3, … 29, Figure 8a), the plate typically slows down. As a result, the continental material has more time to warm up during subduction and gets weaker at a certain depth compared to the situation in models with a prescribed velocity during collision (models 2, 4, … 30, Figure 8b). The weak material tends to return back along the subduction path forming the channel or wedge (compare models 7 and 8, 9 and 10, 13 and 14).

Another important parameter is the thickness of the overriding plate. Sublithospheric relamination is observed only for lithospheric thicknesses of 70 and 90 km. If the overriding plate is too thick (110 km, models 19–22), the continental material cannot subduct under it and/or exhume through it, and rather returns back along the plate interface. In contrast, an extremely thin overriding plate (50 km thick, models 1–6) deforms easily and systematically shows the intracrustal relamination style.

With a prescribed subduction velocity (Figure 8b), the interplay between this velocity and the slab pull is crucial for the situation at the plate interface. Old, and therefore cold and dense oceanic plates (age at the beginning of collision more than ~55 Myr) induce a strong pull which, if not balanced by the subduction velocity, can lead to lithospheric extension and thinning near the trench (e.g., model 12). As a result, a weak zone along the plate interface forms which later permits the exhumation of the subducted material in the form of the channel or wedge. In the case of younger subducting plates the fore arc does not extend,

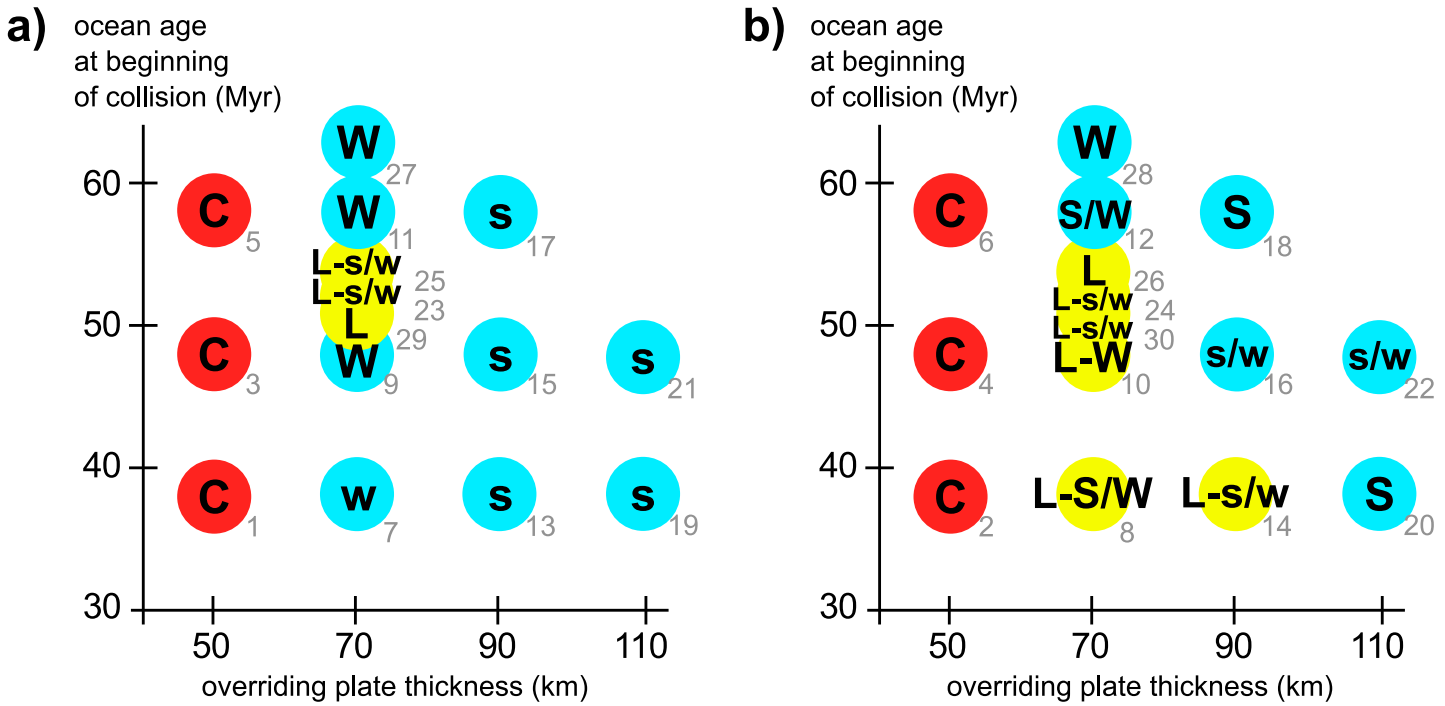

Figure 8. Impact of the overriding plate thickness and of the age of the subducted oceanic plate at the beginning of the collision on the model behavior. (a) Models with a free velocity during continental subduction, (b) models with a fixed velocity during continental subduction. The "C," "L," "S," and "W" correspond to the styles of evolution defined in section 3.3 and noted in the last column of Table 3. Gray index is the model ID. in Table 3. Models 1–30 are shown. In these models only the following parameters vary: duration of convergence condition, initial ocean age and length, velocity of subduction, and thickness of the overriding plate.

and the continental material subducts deeper beneath the overriding plate leading to the sublithospheric relamination (e.g., models 8 and 10).

The age of the oceanic plate at the beginning of collision shown in Figure 8 depends on its initial age, length of the oceanic domain and on the velocity of subduction. The interplay between these parameters is however further complicated due to phase transitions in the mantle, rate-dependent rheology, and other factors. As a result, the models with a higher velocity and/or a narrower ocean behave somewhat differently compared to the main group (models 1–22), and tend to show the sublithospheric relamination even for a free velocity of collision (models 23, 25, and 29).

The strong impact of the age of the subducting plate on the situation near the plate interface is probably related to the fixed position of the overriding plate as documented in models 31–33. If the overriding plate can move freely (model 31), the trench position can adjust to the stress state, extension near the trench does not occur leading to the sublithospheric relamination. A similar behavior is observed if the velocity of convergence is divided between the subducting (3 cm yr^{-1}) and overriding plates (1 cm yr^{-1}) (model 32). The influence of the boundary conditions was further tested by shifting the initial position of the plate interface 200 km to the left (model 33). This leads to a slight change in the subducting plate geometry, reduction of the extension near the trench, and its early closure and development of the sublithospheric relamination style. Nonintuitively, also a thin and warm subducting continental plate (70 km, model 34) promotes relamination. This can be related to easier separation (delamination) of the continental crust from the subducting plate during the change from oceanic to continental subduction.

In addition, we tested the effect of melt-induced weakening which is necessary for penetration of the relaminant through the overriding plate lithosphere. This is shown in model 35, which has the same parameters as model 8 except for the factor $\lambda_m = 10^{-2}$. In this model, the continental material flows horizontally beneath the lithosphere, but no exhumation through the lithosphere occurs until 40 Myr of evolution.

However, reduction of the melt weakening affects also earlier evolution. It is namely in the models with an old oceanic plate where extensional forces lead to lithospheric thinning in the trench region (e.g., model 12).

If we reduce the melt weakening in such a model ($\lambda_m = 10^{-2}$), the plate contact remains closed and extension occurs further within the overriding plate in the magmatic arc region. The continental material then exhumes through this region (model 36).

In the main group of models, we assume that the subducting felsic continental crust (material M3) has a solidus temperature 200 K higher than the sediments (material M2). This assumption reflects the rather dry composition of this crust. In model 37 we use the same (low) solidi for both materials, while other parameters are the same as in model 8. This modification leads to earlier melting and exhumation of the subducted continental material, but the general behavior of the model remains unchanged. The amount of extracted melt X_m is up to 30%, similar as in model 8 (Figure 4).

The last parameter tested here is the thickness of the lower crust of the overriding plate. A thin lower crust (5 km instead of 10 km) effectively reduces the strength of the plate. It may then behave similar to the models with a thin overriding plate, where the crust thickens homogeneously, the lithosphere bends, and the intracrustal relamination occurs (model 38).

4. Discussion

4.1. Key Parameters and Relamination Dynamics

Based on the modeling results, we summarize the main factors causing the occurrence of different evolution styles in Figure 9a.

1. Continuous fast convergence during continental collision favors the development of the sublithospheric relamination style, because only a cold and therefore high-viscosity material can be dragged by the subducting plate to a significant depth. Besides that, the overriding plate lithosphere has to be relatively thin to allow the material to reach its bottom, spread beneath it, and later exhume through it. Weakening of the overriding plate by uprising melt is essential to open the exhumation path for the relaminant.
2. A weak zone near the plate interface promotes return of the subducted material in a subduction channel or wedge. The weakening can result from warming up during slow subduction, or from extension due to strong slab pull by the oceanic plate. The wedge may however develop also in compressional setting where the subduction of the continental crust is restricted.
3. The intracrustal relamination style occurs only if the crust of the overriding plate is very weak. This can result from its predominantly felsic composition or due to an elevated thermal regime.

Figure 9b further illustrates the dynamics of the subduction–relamination process. The evolution begins with oceanic subduction which crucially affects the state of the mantle and lithosphere of the overriding plate as well as the character of the plate interface. Fluids, melt and potentially thermal weakening above the subduction zone modify the location of the weak zone in the mantle which can later host the subducted continental crust.

During oceanic subduction the plate forces ("push" versus "pull" in Figure 9b) can be balanced or induce extensional or compressional stress transmitted to the overriding plate. These forces may lead to lithospheric thinning near the trench, disruption of the overriding plate near the arc or, in contrast, thrusting. After the onset of continental subduction and collision, compression usually prevails and diminishes only after a significant slowdown of the plate convergence.

The subducting crust warms up and weakens as it reaches greater depths with higher ambient temperature. The weak material can flow easily and spreads into a weak horizon available — in the crust (point "C") or mantle (point "L"). If no such horizon is accessible, the material returns along the subducting plate and forms the channel or wedge.

The volume of the crust subducted beneath the lithosphere and the related buoyancy can be significant. A modest estimate of the buoyancy of a 100 km long, 10 km thick body of continental crust is of the order of 10^{12} Nm^{-1} and therefore nearly comparable to the plate forces. As soon as the buoyancy balances the compression due to collision, the exhumation path for the relaminant opens.

The location where exhumation takes place depends on the timing of the change of the force balance, lateral position of the relaminant, and on the site and amount of weakening. The weakening can be provided by melting in the arc region related to oceanic subduction (point "LA") or by melting of the relaminant itself mainly at its tip (point "LB"). If there was no melt weakening of the lithosphere, its strength would be significantly

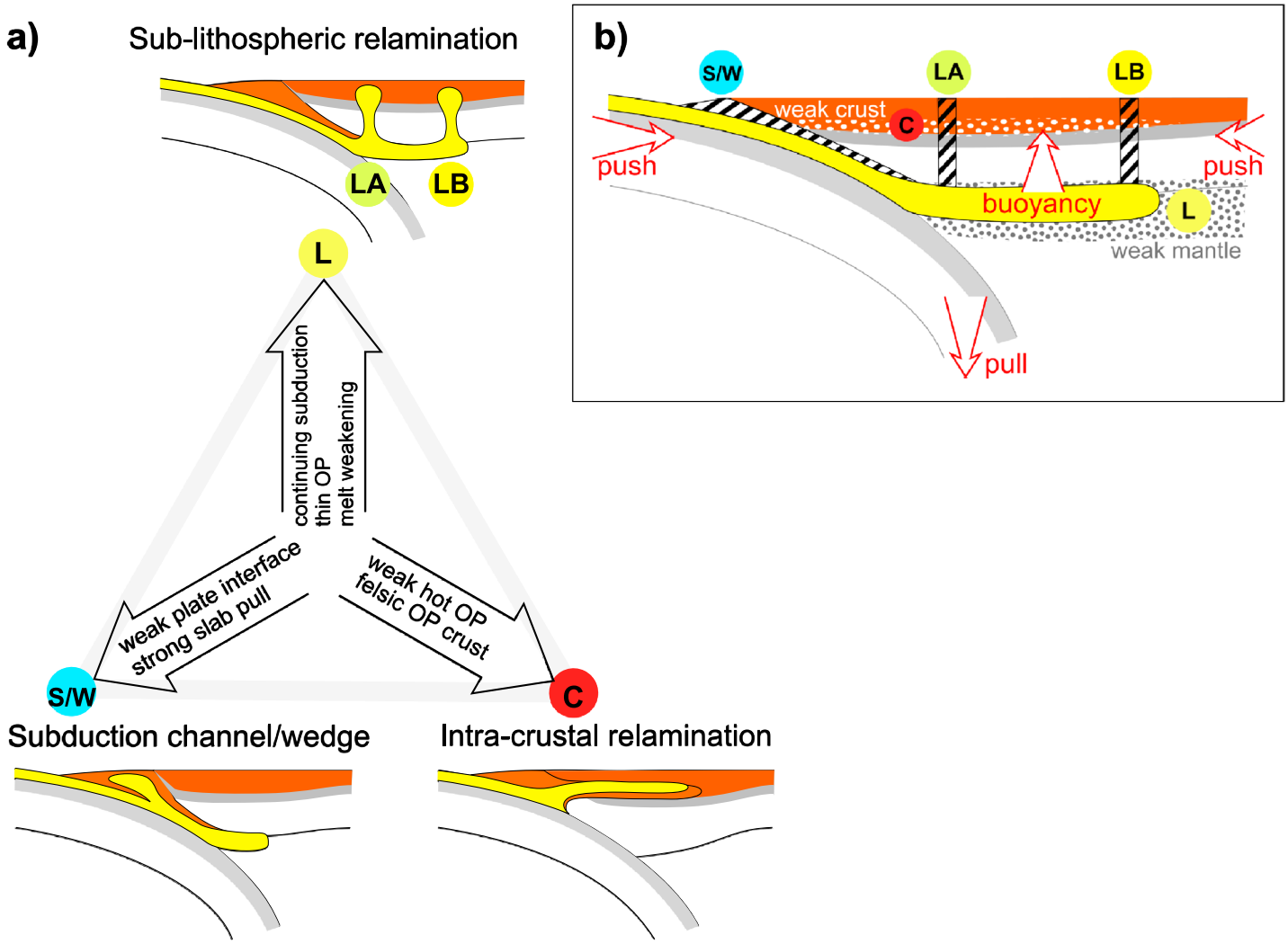

Figure 9. (a) Three end-member styles of evolution and parameters governing their occurrence. (b) Sketch of relamination dynamics. Main rheologically weak horizons—middle crust and sublithospheric mantle—are dotted. Zones of localized weakening that can be used as exhumation paths (along plate interface, near magmatic arc, and above the relaminant tip) are hatched. OP = overriding plate; C = intracrustal relamination; L = sublithospheric relamination; LA = exhumation near the arc; LB = exhumation in the back arc; S/W = formation of the subduction channel or collisional wedge.

higher and the relaminant exhumation would be delayed or prohibited. In some cases the weakest path for exhumation is along the plate interface (point "S/W"), even if it is far from the center of the buoyant felsic body.

In summary, the motion of the subducted felsic crust (the relaminant) is governed by its buoyancy and by the forcing due to the plate motion. It is restricted by the surrounding material and by the viscosity of the relaminant itself. For exhumation it can use previously weakened zones, but its own melting and subsequent melt migration provides another efficient mechanism of weakening.

4.2. Model Simplifications and Restrictions

The presented results depend on many parameters as well as on the general model setup. Here we discuss possible effects of the adopted approach on the results.

4.2.1. Plate Velocity and Boundary Conditions

The choice of appropriate boundary conditions as an approximation of the interaction between the model and the surrounding space is a challenging issue in the modeling of tectonic processes. We test different kinematic conditions and show their effect on the resulting geometry of the subduction zone and the character of the plate interface. In models with a fixed overriding plate, the dip of the subducting slab is mostly vertical, in contrast to natural observations. An inclined slab can be obtained in models with a moving overriding plate (models 31 and 32), but it may also occur when a larger model domain is used (Chertova et al.,

2012). The slab inclination may affect the amount of weakening of the mantle wedge and lithosphere above. For an inclined slab we expect a broader magmatic arc and less focused weakening.

Regarding the subducting plate motion, we can either prescribe its velocity or assume free subduction. The prescribed plate velocity mimics the situation when the subduction dynamics are governed by ridge push or by external forces that may result from the three-dimensional character of the subduction. The resulting (im)balance between the subduction velocity and the slab pull can cause either extension and fore-arc thinning or compression and thrusting. In contrast, free subduction neglects the three dimensionality of the problem and may overestimate the effect of phase transitions on the subduction velocity. In nature there is an interplay between ridge push, slab pull, mantle drag, and other (possibly non-2-D) forces. It is also clear that the situation in real subduction-collision zones may evolve with time. By adding such complexities into the model we could obtain a hybrid development with, for example, alternating compressional and extensional stages.

4.2.2. Slab Detachment

The tested model cases show continuous continental convergence, even if a free motion of plates during collision is prescribed. In that case, the convergence slows down but it is still significant, typically faster than 1 cm yr^{-1}. Such continuation of convergence is observed in the collision between India and Asia (e.g., Guillot et al., 2003). However, cessation of subduction after continental collision and related detachment of the subducted slab is more common (e.g., Andersen et al., 1991). In general, the latter behavior is difficult to obtain in models with relamination (e.g., Magni et al., 2013; Ueda et al., 2012), where the light continental material separates from the subducting plate and therefore does not contribute to its buoyancy. The buoyancy might be increased if a strongly depleted and therefore very light continental root was assumed.

A weak mantle rheology and/or efficient mechanism of weakening and necking of the slab is required to obtain slab detachment (Burkett & Billen, 2009; Duretz et al., 2011). The weakening is provided by stress-dependent Peierls creep in our models, but in our setup it is not sufficient to produce slab detachment. A stronger weakening can result from grain size-sensitive creep in combination with a stress-dependent grain size (e.g., Bercovici & Ricard, 2012).

4.2.3. Plate Interface and Overriding Plate Deformation

The interface between the plates is prescribed somewhat artificially in the model and its properties may affect the model evolution in a very complex manner. For example, viscosity along the interface affects the evolution of the subduction dip (Čížková & Bina, 2013). In some configurations, a rheologically weak plate interface can lead to localization of extension in this region, while a strong interface and a weak overriding plate may induce opening of the back arc (Vogt et al., 2012).

The back-arc opening is not reproduced in our models, probably because of insufficient weakening and lateral uniformity of the overriding plate. If the weak back arc was present, it may provide an alternative path for relaminant exhumation. In addition, the depth of the weak horizon and horizontal flow below lithosphere would be reduced.

4.2.4. Hydration and Melting, Crustal Structure

Hydration and melting are crucial processes during subduction and collision. Hydration reduces the viscosity of the plate interface during subduction. In our model, only a thin layer of mantle above the subducting crust is hydrated, and therefore an overall weakening of the mantle wedge above the subduction zone is not achieved. In this respect, the model is in line with the magmatic-arc formation via mixed sedimentary plumes (Marschall & Schumacher, 2012). The contrasting commonly invoked scenario (e.g., Arcay et al., 2005; Iwamori, 1998) including diffuse hydration of the mantle wedge and related weakening would probably favor relami-

nation at the expense of exhumation near the trench. However, it may also cause more melting and therefore intensive weakening and deformation of the overriding plate during oceanic subduction. As demonstrated in models 38 and 39, a weak overriding plate can inhibit subduction of the felsic continental crust beneath the lithosphere.

Melting and melt extraction are essential for exhumation of the relaminant through the overriding-plate lithosphere. In our model, the extracted melt is assumed to weaken the whole column of material above the region of extraction. As a result, the level of emplacement of the relaminant in the crust is too shallow. The level of emplacement as well as the small-scale deformation of the crust in general may not be well reproduced by our models, because we largely neglect the heterogeneity of the crust. In a more complex model, layered crustal structure and inherited weak zones may perturb the path of the melt, as well as that of the exhuming felsic rocks. As a result small-scale upwellings may develop in addition to the main diapir.

Parameterization of melting as well as melt extraction and emplacement processes may have significant effects on relamination processes by changing geometry and dynamics of crustal and lithospheric weakness zones induced by magmatic processes (e.g., Vogt et al., 2012). Similarly, variations in the density of subducted felsic crust due to compositional effects and/or melting can strongly affect dynamics of relaminants and may potentially cause foundering and sinking of high-density residues from melts extraction into the mantle (Hacker et al., 2011).

4.3. Relamination Styles in Nature and Models

The evolutionary styles described above (subduction channel or collisional wedge, sublithosperic and intracrustal relamination) represent end-members of collisional tectonics that can be depicted in nature. The most prominent natural examples of these tectonic styles are summarized in this section. In addition, we compare the parameters typical of the different modeled styles and the corresponding properties of natural orogens.

4.3.1. Subduction Channel and Collisional Wedge

The return of deeply buried continental crust in a subduction channel or wedge is the most common mode of continental collision (e.g., Platt, 1993). The characteristic feature of this orogenic style is predominantly eclogite-facies metamorphism of the felsic continental crust as it was described in the Scandinavian Caledonides (e.g., Austrheim & Griffin, 1985), Dabie Shan (Hacker et al., 2004), Saxothuringian wedge in the Bohemian Massif (Konopásek & Schulmann, 2005), or the Alps (Chopin, 1984). In the Caledonides the backflow occurred by nappe stacking triggered by eclogitization of Grenville aged granulites (Jolivet et al., 2003) followed by midcrustal extensional shearing. The latter event resulted from the detachment of a significant part of the subducted lithosphere and rebound of the rest of the buoyant plate (Andersen et al., 1991). As a consequence, the thermally weakened crust became redistributed beneath the crustal lid thereby producing giant extension at upper-crustal levels (Milnes & Koyi, 2000).

The subduction channel model was also proposed to explain exhumation of UHP continental rocks in the Variscan Saxothuringian belt. Like in the Caledonides, the exhumation of HP rocks is explained by generalized eduction of crust after slab detachment (Willner et al., 2002) or imbrication of subducted crust and its exhumation in form of crustal nappes (Konopásek & Schulmann, 2005). In contrast, the exhumation of HP continental rocks in the Alpine orogen shows dynamics of a collisional wedge (Allemand & Lardeaux, 1997; Platt, 1993) where the scrapped sheets of continental crust return in a form of thin nappes.

The models presented in this work show that backflow is a viable mode of crustal exhumation under a variety of model parameters. In addition we suggest that neither the scraping of the subducting plate nor the slab detachment and associated rebound are necessary. On the contrary, even deeply relaminated crust can return to the surface and form a thick wedge composed of slices subducted to a variable depth.

4.3.2. Sublithospheric Relamination

The sublithospheric relamination is less well constrained by geological studies. It resembles scenarios proposed to explain collisional dynamics of the Variscan belt in the Bohemian Massif (Behr et al., 1984; Massonne, 2001) or formation of the Tibetan Plateau (Chemenda et al., 2000; Hacker et al., 2011). The common characteristics for both these orogens are the presence of HP felsic granulites and Mg-K magmas (Maierová et al., 2016). In the European Variscan belt the felsic HP granulites crosscut the upper plate in the form of domal structures (Schulmann et al., 2009, 2014), while in central Tibet they occur predominantly as xenoliths trapped by Mg-K volcanites (e.g., Hacker et al., 2000, 2005). However, India-Asia collision in Pamir is characterized by exhumation of granulite facies rocks in the form of giant crustal gneiss domes similar to the Bohemian Massif

(Rutte et al., 2017; Stübner et al., 2013). In the Variscan belt the relaminated crust is exhumed in the arc region (Franěk et al., 2011) and along the boundary between the orogenic root (former back arc) and the more distant continental lithosphere unaffected by deformation (Štípská et al., 2004).

According to the models the sublithospheric relaminant can be exhumed in the previously weakened domain of the magmatic arc where it forms a bulge separating the fore-arc and back-arc regions. Alternatively, if the arc weakening is not efficient enough or its timing is not appropriate, the relaminant tunnels horizontally beneath the mantle lithosphere (cf. Kusbach et al., 2015; Schulmann et al., 2014). The subsequent exhumation occurs far from the arc domain in a region of intensive relaminant melting and transfer of magma through the mantle lithosphere. This magma no longer has the characteristics of arc plutonism but may correspond to Mg-K magmatism as proposed by Janousek and Holub (2007) and Lexa et al. (2011). The depth to which the relaminant ascends is mainly controlled by the rheological structure of the overriding plate. The relaminant tends to spread spontaneously below the strong lithosphere and later inside the low-viscosity ductile crust below the stronger brittle/plastic middle to upper crust. A similar effect is observed during magma intrusion into the crust (e.g., Gerya & Burg, 2007; Keller et al., 2013; Schubert et al., 2013). The relaminant emplacement also resembles the buoyancy-driven flattening of exhumed HP material arrested by the Moho as predicted in Norwegian Caledonides (Walsh & Hacker, 2004).

Previous tectonic and numerical models for the exhumation of HP rocks in the Bohemian Massif and Tibet focused on crustal deformation (e.g., Beaumont et al., 2001; Maierová et al., 2016; Schulmann et al., 2014). The relaminant, if present, was assumed to flow just underneath the crust from where it vertically exhumed to the middle crust. In our models the relaminant flows deeper at the level where the lithosphere changes into the weak asthenosphere. However, the level of its subsequent emplacement in the crust is practically independent of its previous path through the mantle, because it depends mainly on the density and viscosity of the crust and the relaminant. According to geological evidence and crustal-scale models, the middle crust then flows horizontally toward the flank of the orogen where the high-grade rocks are exhumed due to focused erosion. This evolutionary stage is missing in our models and a more detailed setup would probably be necessary to reproduce it.

Our models show that subduction of a young oceanic plate and subsequent quick continental subduction under a thin overriding plate are required to cause sublithospheric relamination. These requirements are met in both of the most typical examples: the European Variscan orogen and Tibet. For the former, high plate velocities are deduced from existing paleomagnetic data (Edel et al., 2013) and geological observations suggesting a short time lag between underthrusting of continental crust, formation of granulites, and their exhumation to the surface (Lexa et al., 2011). In Tibet, high velocities of plates are deduced from paleomagnetism, the distribution of magnetic anomalies in the Indian ocean (Patriat & Achache, 1984), and Global Positioning System data (Zhang et al., 2004). The overriding plate was thin in both Variscan and Tibetan orogens. This is due to their long precollisional history characterized by the formation of back-arc and arc regions established in the upper-plate continental crust (Guillot & Replumaz, 2013; Schulmann et al., 2014).

4.3.3. Intracrustal Relamination

The intracrustal relamination is so far not described in the geological literature. To a certain degree it resembles the models by Beaumont et al. (2001) where the weak lower and upper plate crust become mixed in one orogenic system. These models were applied to classical collisional systems such as the Grenville or Himalaya orogens (Beaumont et al., 2001; Jamieson et al., 2007) and involve horizontal channel flow within the middle crust. This channel is later exhumed due to tectonic forces combined with focused erosion, which is a factor missing in our models.

The main prerequisite for intracrustal relamination to occur in the model is an extreme weakness of the upper-plate crust, which can result from its unusual lithological composition or a high thermal regime. The conditions for intracrustal relamination are hardly attainable in the modern plate tectonic framework which is characterized by a duality of high-pressure–low-temperature subductional and high-temperature–low-pressure arc and back-arc type metamorphism (Brown, 2006). However, high-temperature conditions in the upper plate are met in the Precambrian ultrahot orogens such as the Pan-African orogenic belt or various orogenic systems related to amalgamation of Gondwana (Chardon et al., 2009). These systems show medium-pressure (ultra)high-temperature metamorphic conditions and general weakness of the crust that fit to the thermal and rheological properties required by the intracrustal relamination model.

4.3.4. Mixed Styles

A mixed style of evolution can be depicted in both the European Variscan belt and the Himalayan–Tibetan orogen. The former orogen reveals a range of arguments for sublithospheric relamination preceding exhumation of HP granulites in the arc region (Franěk et al., 2011) and at the boundary of the former back arc (Moldanubian root) and the remaining continent (Štípská et al., 2004). In addition it is characterized by the large-scale extrusion of HP rocks along the margin of the subducting Saxothuringian plate (Franke & Stein, 2000; Konopásek & Schulmann, 2005). Such a combination of exhumation styles is reproduced in our models (e.g., model 8). In addition, these models predict that the exhumation along the plate interface postdates the exhumation through the orogenic lithosphere, which is in agreement with dating of UHP rocks by Massonne et al. (2007).

Similar evolution is reported in the Tibetan-Himalayan orogen (Kali et al., 2010, Guilmette et al., 2011, and references therein), where the HP granulites first formed 40–30 Myr ago far from the plate interface. In contrast, these rocks are exhumed in crustal domes in Southern Tibet close to the plate interface or within a crustal channel 20–3 Myr ago.

Diachronous exhumation and contrasting metamorphic conditions were also deduced for the HP rocks in the northwestern and eastern Himalaya (Warren et al., 2011, and references therein). In the northwest, the peak temperatures are lower and exhumation occurred earlier (~50 Myr ago) than in the east (~20–13 Myr ago). In our view this may correspond to a change from wedge-like to relamination tectonics.

5. Conclusions

The presented thermomechanical models of continental subduction and collision show three contrasting styles of behavior:

1. Return of the subducted crust along the plate interface in the form of the collisional wedge or the hot channel;
2. Flow beneath the lithosphere and vertical exhumation into the overriding plate crust near the magmatic arc or in the back-arc region called here sublithospheric relamination, and
3. Direct nearly horizontal flow into the overriding plate crust called here intracrustal relamination.

Each of these modeled styles have their natural counterparts, for example, in the Caledonides, Alpes, Variscan belt, Himalaya, and possibly pre-Cambrian orogens. We show that the values of the parameters required to obtain the three styles in the models mostly comply with the characteristics of their respective examples in nature. In particular, the sublithospheric relamination is likely in orogens formed by young, thin and quickly colliding plates.

Our study is only a single step in understanding the dynamics of relamination, and future studies shall test other important parameters and may even bring in other styles of evolution. Nevertheless, we show that the flow of crustal material underneath the lithosphere and then back to the crust is feasible and that such a subduction-relamination history can be obtained for a wide range of conditions.

Appendix A: Governing Equations, Rheology, and Surface Processes

We assume a compressible material with negligible inertia described by the following equations of conservation of momentum and mass:

$$\frac{\partial v_x}{\partial x} + \frac{\partial v_y}{\partial y} = \mathrm{div}_{\mathrm{melt}}, \tag{A1}$$

$$\frac{\partial \sigma_{xx}}{\partial x} + \frac{\partial \sigma_{xy}}{\partial y} = \frac{\partial P}{\partial x}, \tag{A2}$$

$$\frac{\partial \sigma_{yx}}{\partial x} + \frac{\partial \sigma_{yy}}{\partial y} = \frac{\partial P}{\partial y} - g\rho_{\mathrm{eff}}, \tag{A3}$$

where x and y are Eulerian coordinates (y increases downward), v_i are components of the velocity vector, $\mathrm{div}_{\mathrm{melt}}$ is a local volumetric effect of melt extraction/emplacement, σ_{ij} are components of the deviatoric

stress tensor, P is the pressure, $g = 9.81$ m s^{-2} is the gravity acceleration, and ρ_{eff} is the effective density. The conservation of energy is expressed by the following equation:

$$\rho_{\text{eff}} c_p \frac{\mathrm{D}T}{\mathrm{D}t} = \frac{\partial}{\partial x}\left(k\frac{\partial T}{\partial x}\right) + \frac{\partial}{\partial y}\left(k\frac{\partial T}{\partial y}\right) + H_r + H_a + H_s, \tag{A4}$$

where c_p is the heat capacity, T is the temperature, t is the time, and k is the thermal conductivity. H_r, H_a, and H_s are radiogenic, adiabatic, and shear heat sources, respectively:

$$H_r = \text{constant}, \tag{A5}$$

$$H_a = -T\alpha\rho v_y g, \tag{A6}$$

$$H_s = \sigma_{xx}\dot{\epsilon}_{xx} + 2\sigma_{xy}\dot{\epsilon}_{xy} + \sigma_{yy}\dot{\epsilon}_{yy}, \tag{A7}$$

where α is the thermal expansivity and $\dot{\epsilon}_{ij}$ are components of the deviatoric strain rate tensor:

$$\dot{\epsilon}_{xx} = \frac{1}{2}\left(\frac{\partial v_x}{\partial x} - \frac{\partial v_y}{\partial y}\right), \tag{A8}$$

$$\dot{\epsilon}_{xy} = \frac{1}{2}\left(\frac{\partial v_x}{\partial y} + \frac{\partial v_y}{\partial x}\right), \tag{A9}$$

$$\dot{\epsilon}_{yy} = \frac{1}{2}\left(\frac{\partial v_y}{\partial y} - \frac{\partial v_x}{\partial x}\right). \tag{A10}$$

The relationship between the deviatoric stress and strain rate tensors is expressed via the effective viscosity η_{eff}:

$$\sigma_{xx} = 2\eta_{\text{eff}}\dot{\epsilon}_{xx}, \tag{A11}$$

$$\sigma_{xy} = 2\eta_{\text{eff}}\dot{\epsilon}_{xy}, \tag{A12}$$

$$\sigma_{yy} = 2\eta_{\text{eff}}\dot{\epsilon}_{yy}, \tag{A13}$$

The effective viscosity is a result of a combination of different deformation mechanisms:

1. brittle deformation (specified in the main text),
2. dislocation creep:

$$\eta_{\text{dis}} = \frac{1}{2}A^{\frac{-1}{n}}\dot{\epsilon}_{\text{II}}^{\frac{1-n}{n}}\exp\left(\frac{E_A + V_A P}{nRT}\right), \tag{A14}$$

   where $\dot{\epsilon}_{\text{II}} = \sqrt{1/2\sum_{ij}\dot{\epsilon}_{ij}\dot{\epsilon}_{ij}}$ is the second invariant of the deviatoric strain rate tensor, A is the prefactor, n is the stress exponent, E_A is the activation energy, V_A is the activation volume, and R is the gas constant,
3. diffusion creep:

$$\eta_{\text{dif}} = \frac{1}{2}A^{-1}\exp\left(\frac{E_A + V_A P}{RT}\right), \tag{A15}$$

   where the grain size is assumed to be constant,
4. Peierls creep:

$$\eta_{\text{pei}} = A^{-1}\sigma_{\text{II}}^{-1}\exp\left(\frac{E_A + V_A P}{RT}\left(1 - \frac{\sigma_{\text{II}}}{\sigma_{\text{pei}}}\right)^2\right), \tag{A16}$$

Table A1
Creep Parameters

Flow law	Type	A ($Pa^{-n}\ s^{-1}$)	n	E_A (kJ mol^{-1})	V_A ($m^3\ mol^{-1}$)	σ_{pei} (MPa)	References
Wet quartz	dislocation	$5.1 \cdot 10^{-18}$	2.3	154	$3 \cdot 10^{-6}$	—	a
Anorthite	dislocation	$2.1 \cdot 10^{-23}$	3.2	238	$8 \cdot 10^{-6}$	—	a
Dry olivine	dislocation	$2.4 \cdot 10^{-16}$	3.5	540	$20 \cdot 10^{-6}$	—	b
Dry olivine	diffusion	$1.9 \cdot 10^{-11}$	—	300	$4 \cdot 10^{-6}$	—	b
Wet olivine	dislocation	$3.9 \cdot 10^{-15}$	3.0	430	$10 \cdot 10^{-6}$	—	b
Wet olivine	diffusion	$1.2 \cdot 10^{-11}$	—	240	$4 \cdot 10^{-6}$	—	b
All mantle rocks	Peierls	$6.3 \cdot 10^{-5}$	2.0	540	$20 \cdot 10^{-6}$	9.1	b,c

[a]Ranalli (1995). [b]Karato and Wu (1993), where prefactor A is calculated for grain size 1 mm, $m = 2.5$, Burgers vector length 0.5 nm and shear modulus 80 GPa. [c]Evans and Goetze (1979) and Katayama and Karato (2008).

σ_{pei} is the Peierls stress.

Parameter values are specified in Table A1. The deformation mechanisms are combined according to equations (2) and (3) in the main text.

Erosion and sedimentation are expressed by a transport equation:

$$\frac{\partial y_e}{\partial t} = v_y - v_x \frac{\partial y_e}{\partial x} - v_s + v_e \tag{A17}$$

where y_e is the vertical position of the surface, v_x, v_y are the horizontal and vertical components of the material velocity vector, v_s, and v_e are the sedimentation and erosion parameters, respectively:

$$\begin{aligned} v_s = 0,\ v_e = v_{e0} \text{ for } y \le 18 \text{ km}, \\ v_s = v_{s0}, v_e = 0 \text{ for } y > 18.5 \text{ km}, \end{aligned} \tag{A18}$$

where $v_{e0} = 3$ mm yr^{-1} is the erosion parameter, $v_{s0} = 0.3$ mm yr^{-1} is the sedimentation parameter, and $y = 18.5$ km is the initial sea level.

Acknowledgments
This work is a contribution to the project "DSP-Tibet" ANR-13-BS06-012-01 funded by the Agence Nationale de la Recherche. We acknowledge financial support through the GAČR (Grantová Agentura České Republiky) project 17-22207S. We thank Fabio A. Capitanio, Bradley Hacker, and the Editor Jeroen van Hunen for their constructive comments that helped to enhance the quality of the manuscript. We thank Ondrej Lexa for inspiring discussions and Stephen Collett for careful reading and corrections of the manuscript. Supplementary figures showing the results of all presented model cases are available here: "https://doi.org/10.6084/m9.figshare.5426512.v1".

References

Allemand, P., & Lardeaux, J.-M. (1997). Strain partitioning and metamorphism in a deformable orogenic wedge: Application to the Alpine belt. *Tectonophysics*, *280*(1–2), 157–169.

Andersen, T. B., Jamtveit, B., Dewey, J. F., & Swensson, E. (1991). Subduction and eduction of continental crust: Major mechanisms during continent-continent collision and orogenic extensional collapse, a model based on the south Norwegian Caledonides. *Terra Nova*, *3*(3), 303–310.

Arcay, D., Tric, E., & Doin, M.-P. (2005). Numerical simulations of subduction zones: Effect of slab dehydration on the mantle wedge dynamics. *Physics of the Earth and Planetary Interiors*, *149*(1), 133–153.

Artemieva, I. M. (2006). Global 1 × 1 thermal model TC1 for the continental lithosphere: Implications for lithosphere secular evolution. *Tectonophysics*, *416*(1), 245–277.

Austrheim, H., & Griffin, W. L. (1985). Shear deformation and eclogite formation within granulite-facies anorthosites of the Bergen Arcs, western Norway. *Chemical Geology*, *50*(1), 267–281.

Beaumont, C., Jamieson, R. A., Nguyen, M., & Lee, B. (2001). Himalayan tectonics explained by extrusion of a low-viscosity crustal channel coupled to focused surface denudation. *Nature*, *414*(6865), 738–742.

Behn, M. D., Kelemen, P. B., Hirth, G., Hacker, B. R., & Massonne, H.-J. (2011). Diapirs as the source of the sediment signature in arc lavas. *Nature Geoscience*, *4*(9), 641.

Behr, H.-J., Engel, W., Franke, W., Giese, P., & Weber, K. (1984). The Variscan belt in Central Europe: main structures, geodynamic implications, open questions. *Tectonophysics*, *109*(1–2), 15–40.

Bercovici, D., & Ricard, Y. (2012). Mechanisms for the generation of plate tectonics by two-phase grain-damage and pinning. *Physics of the Earth and Planetary Interiors*, *202*, 27–55.

Bittner, D., & Schmeling, H. (1995). Numerical modelling of melting processes and induced diapirism in the lower crust. *Geophysical Journal International*, *123*(1), 59–70.

Brown, M. (2006). Duality of thermal regimes is the distinctive characteristic of plate tectonics since the Neoarchean. *Geology*, *34*(11), 961–964.

Burkett, E. R., & Billen, M. I. (2009). Dynamics and implications of slab detachment due to ridge-trench collision. *Journal of Geophysical Research*, *114*, B12402. https://doi.org/10.1029/2009JB006402

Castro, A., Vogt, K., & Gerya, T. (2013). Generation of new continental crust by sublithospheric silicic-magma relamination in arcs: A test of Taylor's andesite model. *Gondwana Research*, *23*(4), 1554–1566.

Chardon, D., Gapais, D., & Cagnard, F. (2009). Flow of ultra-hot orogens: A view from the Precambrian, clues for the Phanerozoic. *Tectonophysics*, *477*(3), 105–118.
Chemenda, A. I., Burg, J.-P., & Mattauer, M. (2000). Evolutionary model of the Himalaya–Tibet system: geopoem based on new modelling, geological and geophysical data. *Earth and Planetary Science Letters*, *174*(3), 397–409.
Chertova, M., Geenen, T., van den Berg, A., & Spakman, W. (2012). Using open sidewalls for modelling self-consistent lithosphere subduction dynamics. *Solid Earth*, *3*(2), 313–326.
Chopin, C. (1984). Coesite and pure pyrope in high-grade blueschists of the Western Alps: A first record and some consequences. *Contributions to Mineralogy and Petrology*, *86*(2), 107–118.
Čížková, H., & Bina, C. R. (2013). Effects of mantle and subduction-interface rheologies on slab stagnation and trench rollback. *Earth and Planetary Science Letters*, *379*, 95–103.
Clauser, C., & Huenges, E. (1995). Thermal conductivity of rocks and minerals. In Ahrens, T. J. (Ed.), *Rock physics and phase relations: A handbook of physical constants* (pp. 105–126). Washington, DC: American Geophysical Union.
Crameri, F., Schmeling, H., Golabek, G., Duretz, T., Orendt, R., Buiter, S., … Tackley, P. (2012). A comparison of numerical surface topography calculations in geodynamic modelling: An evaluation of the 'sticky air' method. *Geophysical Journal International*, *189*(1), 38–54.
Ding, L., Kapp, P., Yue, Y., & Lai, Q. (2007). Postcollisional calc-alkaline lavas and xenoliths from the southern Qiangtang terrane, central Tibet. *Earth and Planetary Science Letters*, *254*(1), 28–38.
Duretz, T., Gerya, T. V., & May, D. A. (2011). Numerical modelling of spontaneous slab breakoff and subsequent topographic response. *Tectonophysics*, *502*(1), 244–256.
Dymkova, D., Gerya, T., & Burg, J.-P. (2016). 2D thermomechanical modelling of continent–arc–continent collision. *Gondwana Research*, *32*, 138–150.
Edel, J., Schulmann, K., Skrzypek, E., & Cocherie, A. (2013). Tectonic evolution of the European Variscan belt constrained by palaeomagnetic, structural and anisotropy of magnetic susceptibility data from the Northern Vosges magmatic arc (eastern France). *Journal of the Geological Society*, *170*(5), 785–804.
Evans, B., & Goetze, C. (1979). The temperature variation of hardness of olivine and its implication for polycrystalline yield stress. *Journal of Geophysical Research*, *84*(B10), 5505–5524.
Faccenda, M., Gerya, T. V., & Chakraborty, S. (2008). Styles of post-subduction collisional orogeny: Influence of convergence velocity, crustal rheology and radiogenic heat production. *Lithos*, *103*(1), 257–287.
Franěk, J., Schulmann, K., Lexa, O., Tomek, Č., & Edel, J.-B. (2011). Model of syn-convergent extrusion of orogenic lower crust in the core of the Variscan belt: Implications for exhumation of high-pressure rocks in large hot orogens. *Journal of Metamorphic Geology*, *29*(1), 53–78.
Franke, W., & Stein, E. (2000). Exhumation of high-grade rocks in the Saxo-Thuringian Belt: Geological constraints and geodynamic concepts. *Geological Society, London, Special Publications*, *179*(1), 337–354.
Gerya, T., Perchuk, L., & Burg, J.-P. (2008). Transient hot channels: Perpetrating and regurgitating ultrahigh-pressure, high-temperature crust–mantle associations in collision belts. *Lithos*, *103*(1), 236–256.
Gerya, T. V., & Burg, J.-P. (2007). Intrusion of ultramafic magmatic bodies into the continental crust: Numerical simulation. *Physics of the Earth and Planetary Interiors*, *160*(2), 124–142.
Gerya, T. V., & Yuen, D. A. (2003). Characteristics-based marker-in-cell method with conservative finite-differences schemes for modeling geological flows with strongly variable transport properties. *Physics of the Earth and Planetary Interiors*, *140*(4), 293–318.
Gerya, T. V., Stöckhert, B., & Perchuk, A. L. (2002). Exhumation of high-pressure metamorphic rocks in a subduction channel: A numerical simulation. *Tectonics*, *21*(6), 1056. https://doi.org/10.1029/2002TC001406
Gorczyk, W., Willner, A. P., Gerya, T. V., Connolly, J. A., & Burg, J.-P. (2007). Physical controls of magmatic productivity at Pacific-type convergent margins: Numerical modelling. *Physics of the Earth and Planetary Interiors*, *163*(1), 209–232.
Guillot, S., & Replumaz, A. (2013). Importance of continental subductions for the growth of the Tibetan plateau. *Bulletin de la Société Géologique de France*, *184*(3), 199–223.
Guillot, S., Garzanti, E., Baratoux, D., Marquer, D., Mahéo, G., & De Sigoyer, J. (2003). Reconstructing the total shortening history of the NW Himalaya. *Geochemistry, Geophysics, Geosystems*, *4*(7), 1064. https://doi.org/10.1029/2002GC000484
Guilmette, C., Indares, A., & Hébert, R. (2011). High-pressure anatectic paragneisses from the Namche Barwa, Eastern Himalayan Syntaxis: Textural evidence for partial melting, phase equilibria modeling and tectonic implications. *Lithos*, *124*(1), 66–81.
Hacker, B., Luffi, P., Lutkov, V., Minaev, V., Ratschbacher, L., Plank, T., … Metcalf, J. (2005). Near-ultrahigh pressure processing of continental crust: Miocene crustal xenoliths from the Pamir. *Journal of Petrology*, *46*(8), 1661–1687.
Hacker, B. R., Gnos, E., Ratschbacher, L., Grove, M., McWilliams, M., Sobolev, S. V., … Zhenhan, W. (2000). Hot and dry deep crustal xenoliths from Tibet. *Science*, *287*(5462), 2463–2466.
Hacker, B. R., Ratschbacher, L., & Liou, J. (2004). Subduction, collision and exhumation in the ultrahigh-pressure Qinling-Dabie orogen. *Geological Society, London, Special Publications*, *226*(1), 157–175.
Hacker, B. R., Kelemen, P. B., & Behn, M. D. (2011). Differentiation of the continental crust by relamination. *Earth and Planetary Science Letters*, *307*(3), 501–516.
Hess, P. C. (1989). *Origins of igneous rocks* (336 pp.). Cambridge: Harvard University Press.
Houseman, G., & Molnar, P. (2001). Mechanisms of lithospheric rejuvenation associated with continental orogeny. *Geological Society, London, Special Publications*, *184*(1), 13–38.
Ito, E., Akaogi, M., Topor, L., & Navrotsky, A. (1990). Negative pressure-temperature slopes for reactions forming MgSiO3 perovskite from calorimetry. *Science*, *249*(4974), 1275–1278.
Ito, K., & Kennedy, G. C. (1971). An experimental study of the basalt-garnet granulite-eclogite transition. *The Structure and Physical Properties of the Earth's Crust*, *14*, 303–314.
Iwamori, H. (1998). Transportation of H_2O and melting in subduction zones. *Earth and Planetary Science Letters*, *160*(1), 65–80.
Jamieson, R. A., Beaumont, C., Nguyen, M., & Culshaw, N. (2007). Synconvergent ductile flow in variable-strength continental crust: Numerical models with application to the western Grenville orogen. *Tectonics*, *26*, TC5005. https://doi.org/10.1029/2006TC002036
Janoušek, V., & Holub, F. V. (2007). The causal link between HP-HT metamorphism and ultrapotassic magmatism in collisional orogens: Case study from the Moldanubian Zone of the Bohemian Massif. *Proceedings of the Geologists' Association*, *118*(1), 75–86.
Jarrard, R. D. (1986). Relations among subduction parameters. *Reviews of Geophysics*, *24*(2), 217–284.
Johannes, W. (1985). The significance of experimental studies for the formation of migmatites. In Ashworth, J. R. (Ed.), *Migmatites* (pp. 36–85). Boston, MA: Springer.
Johnston, S. M., Hacker, B. R., & Andersen, T. B. (2007). Exhuming Norwegian ultrahigh-pressure rocks: Overprinting extensional structures and the role of the Nordfjord-Sogn Detachment Zone. *Tectonics*, *26*, TC5001. https://doi.org/10.1029/2005TC001933

Jolivet, L., Faccenna, C., Goffé, B., Burov, E., & Agard, P. (2003). Subduction tectonics and exhumation of high-pressure metamorphic rocks in the Mediterranean orogens. *American Journal of Science*, *303*(5), 353–409.
Kali, E., Leloup, P., Arnaud, N., Mahéo, G., Liu, D., Boutonnet, E., … Li, H. (2010). Exhumation history of the deepest central Himalayan rocks, Ama Drime range: Key pressure-temperature-deformation-time constraints on orogenic models. *Tectonics*, *29*, TC2014. https://doi.org/10.1029/2009TC002551
Karato, S.-I., & Wu, P. (1993). Rheology of the upper mantle: A synthesis. *Science*, *260*(5109), 771–778.
Katayama, I., & Karato, S.-I. (2008). Low-temperature, high-stress deformation of olivine under water-saturated conditions. *Physics of the Earth and Planetary Interiors*, *168*(3), 125–133.
Katsura, T., & Ito, E. (1989). The system Mg_2SiO_4-Fe_2SiO_4 at high pressures and temperatures: Precise determination of stabilities of olivine, modified spinel, and spinel. *Journal of Geophysical Research*, *94*(B11), 15,663–15,670.
Katz, R. F., Spiegelman, M., & Langmuir, C. H. (2003). A new parameterization of hydrous mantle melting. *Geochemistry, Geophysics, Geosystems*, *4*, 1073. https://doi.org/10.1029/2002GC000433
Kay, R. W., & Kay, S. M. (1993). Delamination and delamination magmatism. *Tectonophysics*, *219*(1-3), 177–189.
Kelemen, P., Hanghøj, K., & Greene, A. (2003). One view of the geochemistry of subduction-related magmatic arcs, with an emphasis on primitive andesite and lower crust. *Treatise on Geochemistry*, *3*, 593–659.
Kelemen, P. B., & Behn, M. D. (2016). Formation of lower continental crust by relamination of buoyant arc lavas and plutons. *Nature Geoscience*, *9*, 197–205.
Keller, T., May, D. A., & Kaus, B. J. (2013). Numerical modelling of magma dynamics coupled to tectonic deformation of lithosphere and crust. *Geophysical Journal International*, *195*(3), 1406–1442.
Konopásek, J., & Schulmann, K. (2005). Contrasting Early Carboniferous field geotherms: Evidence for accretion of a thickened orogenic root and subducted Saxothuringian crust (Central European Variscides). *Journal of the Geological Society*, *162*(3), 463–470.
Kusbach, V., Janoušek, V., Hasalová, P., Schulmann, K., Fanning, C. M., Erban, V., & Ulrich, S. (2015). Importance of crustal relamination in origin of the orogenic mantle peridotite-high-pressure granulite association: Example from the Naměšť Granulite Massif (Bohemian Massif, Czech Republic). *Journal of the Geological Society*, *172*, 479–490. https://doi.org/10.1144/jgs2014-070
Lexa, O., Schulmann, K., Janoušek, V., Štípská, P., Guy, A., & Racek, M. (2011). Heat sources and trigger mechanisms of exhumation of HP granulites in Variscan orogenic root. *Journal of Metamorphic Geology*, *29*(1), 79–102.
Little, T., Hacker, B., Gordon, S., Baldwin, S., Fitzgerald, P., Ellis, S., & Korchinski, M. (2011). Diapiric exhumation of Earth's youngest (UHP) eclogites in the gneiss domes of the d'Entrecasteaux Islands, Papua New Guinea. *Tectonophysics*, *510*(1), 39–68.
Magni, V., Faccenna, C., Hunen, J., & Funiciello, F. (2013). Delamination vs. break-off: The fate of continental collision. *Geophysical Research Letters*, *40*, 285–289. https://doi.org/10.1002/grl.50090
Maierová, P., Schulmann, K., Lexa, O., Guillot, S., Štípská, P., Janoušek, V., & Čadek, O. (2016). European Variscan orogenic evolution as an analogue of Tibetan-Himalayan orogen: Insights from petrology and numerical modeling. *Tectonics*, *35*, 1760–1780. https://doi.org/10.1002/2015TC004098
Marschall, H. R., & Schumacher, J. C. (2012). Arc magmas sourced from mélange diapirs in subduction zones. *Nature Geoscience*, *5*(12), 862–867.
Massonne, H.-J. (2001). First find of coesite in the ultrahigh-pressure metamorphic area of the central Erzgebirge, Germany. *European Journal of Mineralogy*, *13*(3), 565–570.
Massonne, H.-J., Kennedy, A., Nasdala, L., & Theye, T. (2007). Dating of zircon and monazite from diamondiferous quartzofeldspathic rocks of the Saxonian Erzgebirge—Hints at burial and exhumation velocities. *Mineralogical Magazine*, *71*(4), 407–425.
Maunder, B., van Hunen, J., Magni, V., & Bouilhol, P. (2016). Relamination of mafic subducting crust throughout Earth's history. *Earth and Planetary Science Letters*, *449*, 206–216.
Milnes, A., & Koyi, H. (2000). Ductile rebound of an orogenic root: Case study and numerical model of gravity tectonics in the Western Gneiss Complex, Caledonides, southern Norway. *Terra Nova*, *12*(1), 1–7.
Mishin, Y. A., Gerya, T. V., Burg, J.-P., & Connolly, J. A. (2008). Dynamics of double subduction: Numerical modeling. *Physics of the Earth and Planetary Interiors*, *171*(1), 280–295.
Nikolaeva, K., Gerya, T. V., & Connolly, J. A. (2008). Numerical modelling of crustal growth in intraoceanic volcanic arcs. *Physics of the Earth and Planetary Interiors*, *171*(1), 336–356.
Patriat, P., & Achache, J. (1984). India–Eurasia collision chronology has implications for crustal shortening and driving mechanism of plates. *Nature*, *311*, 615–621.
Platt, J. (1993). Exhumation of high-pressure rocks: A review of concepts and processes. *Terra Nova*, *5*(2), 119–133.
Poli, S., & Schmidt, M. W. (2002). Petrology of subducted slabs. *Annual Review of Earth and Planetary Sciences*, *30*(1), 207–235.
Ranalli, G. (1995). *Rheology of the Earth*: Springer Science & Business Media.
Rudnick, R., & Gao, S. (2003). Composition of the continental crust, *Treatise on geochemistry* (Vol. 3, 659 pp.). Oxford: Elsevier.
Rutte, D., Ratschbacher, L., Schneider, S., Stübner, K., Stearns, M. A., Gulzar, M. A., & Hacker, B. R. (2017). Building the Pamir-Tibetan Plateau–Crustal stacking, extensional collapse, and lateral extrusion in the Central Pamir: 1. Geometry and kinematics. *Tectonics*, *36*, 342–384. https://doi.org/10.1002/2016TC004293
Schmeling, H., Babeyko, A., Enns, A., Faccenna, C., Funiciello, F., Gerya, T., … van Hunen, J. (2008). A benchmark comparison of spontaneous subduction models—Towards a free surface. *Physics of the Earth and Planetary Interiors*, *171*(1), 198–223.
Schubert, M., Driesner, T., Gerya, T., & Ulmer, P. (2013). Mafic injection as a trigger for felsic magmatism: A numerical study. *Geochemistry, Geophysics, Geosystems*, *14*, 1910–1928. https://doi.org/10.1002/ggge.20124
Schulmann, K., Konopásek, J., Janoušek, V., Lexa, O., Lardeaux, J.-M., Edel, J.-B., … Ulrich, S. (2009). An Andean type Palaeozoic convergence in the Bohemian massif. *Comptes Rendus Geoscience*, *341*(2), 266–286.
Schulmann, K., Lexa, O., Janoušek, V., Lardeaux, J. M., & Edel, J. B. (2014). Anatomy of a diffuse cryptic suture zone: An example from the Bohemian Massif, European Variscides. *Geology*, *42*(4), 275–278. https://doi.org/10.1130/G35290.1
Sizova, E., Gerya, T., & Brown, M. (2012). Exhumation mechanisms of melt-bearing ultrahigh pressure crustal rocks during collision of spontaneously moving plates. *Journal of Metamorphic Geology*, *30*(9), 927–955.
Stübner, K., Ratschbacher, L., Weise, C., Chow, J., Hofmann, J., Khan, J., … Project TIPAGE members (2013). The giant Shakhdara migmatitic gneiss dome, Pamir, India-Asia collision zone: 2. Timing of dome formation. *Tectonics*, *32*, 1404–1431. https://doi.org/10.1002/tect.20059
Tamura, Y., Ishizuka, O., Aoike, K., Kawate, S., Kawabata, H., Chang, Q., … Fiske, R. S. (2010). Missing oligocene crust of the Izu–Bonin arc: Consumed or rejuvenated during collision? *Journal of Petrology*, *51*(4), 823–846.
Štípská, P., Schulmann, K., & Kröner, A. (2004). Vertical extrusion and middle crustal spreading of omphacite granulite: A model of syn-convergent exhumation (Bohemian Massif, Czech Republic). *Journal of Metamorphic Geology*, *22*(3), 179–198.
Turcotte, D., & Schubert, G. (2002). *Geodynamics* (p. 456).

Ueda, K., Gerya, T. V., & Burg, J.-P. (2012). Delamination in collisional orogens: Thermomechanical modeling. *Journal of Geophysical Research*, *117*, B08202. https://doi.org/10.1029/2012JB009144

Vogt, K., Gerya, T. V., & Castro, A. (2012). Crustal growth at active continental margins: Numerical modeling. *Physics of the Earth and Planetary Interiors*, *192*, 1–20.

Walsh, E., & Hacker, B. (2004). The fate of subducted continental margins: Two-stage exhumation of the high-pressure to ultrahigh-pressure Western Gneiss Region, Norway. *Journal of Metamorphic Geology*, *22*(7), 671–687.

Warren, C., Grujic, D., Kellett, D., Cottle, J., Jamieson, R. A., & Ghalley, K. (2011). Probing the depths of the India-Asia collision: U-Th-Pb monazite chronology of granulites from NW Bhutan. *Tectonics*, *30*, TC2004. https://doi.org/10.1029/2010TC002738

Warren, C. J., Beaumont, C., & Jamieson, R. A. (2008). Formation and exhumation of ultra-high-pressure rocks during continental collision: Role of detachment in the subduction channel. *Geochemistry, Geophysics, Geosystems*, *9*, Q04019. https://doi.org/10.1029/2007GC001839

Willner, A., Sebazungu, E., Gerya, T., Maresch, W., & Krohe, A. (2002). Numerical modelling of PT-paths related to rapid exhumation of high-pressure rocks from the crustal root in the Variscan Erzgebirge Dome (Saxony/Germany). *Journal of Geodynamics*, *33*(3), 281–314.

Yin, A., Manning, C. E., Lovera, O., Menold, C. A., Chen, X., & Gehrels, G. E. (2007). Early Paleozoic tectonic and thermomechanical evolution of ultrahigh-pressure (UHP) metamorphic rocks in the northern Tibetan Plateau, northwest China. *International Geology Review*, *49*(8), 681–716.

Zhang, P.-Z., Shen, Z., Wang, M., Gan, W., Bürgmann, R., Molnar, P., … Xinzhao, Y. (2004). Continuous deformation of the Tibetan Plateau from global positioning system data. *Geology*, *32*(9), 809–812.

Zhu, G., Gerya, T. V., Yuen, D. A., Honda, S., Yoshida, T., & Connolly, J. A. (2009). Three-dimensional dynamics of hydrous thermal-chemical plumes in oceanic subduction zones. *Geochemistry, Geophysics, Geosystems*, *10*, Q11006. https://doi.org/10.1029/2009GC002625

Erratum

In the originally published version of this article, initial thicknesses of the layers M3 and M4 as stated in the caption for Figure 1 were incorrect (different than in the actual model setup). The correct thicknesses are as follows: M3: 15 km, M4: 20 km. This has since been corrected, and this version may be considered the authoritative version of record.